

The tectonic cause of mass extinctions and the genomic contribution to biodiversification

Dirson Jian Li

Department of Applied Physics, Xi'an Jiaotong University, Xi'an 710049, China

Abstract

Despite numerous mass extinctions in the Phanerozoic eon, the overall trend in biodiversity evolution was not blocked and the life has never been wiped out. Almost all possible catastrophic events (large igneous province, asteroid impact, climate change, regression and transgression, anoxia, acidification, sudden release of methane clathrate, multi-cause etc.) have been proposed to explain the mass extinctions. However, we should, above all, clarify at what timescale and at what possible levels should we explain the mass extinction? Even though the mass extinctions occurred at short-timescale and at the species level, we reveal that their cause should be explained in a broader context at tectonic timescale and at both the molecular level and the species level. The main result in this paper is that the Phanerozoic biodiversity evolution has been explained by reconstructing the Sepkoski curve based on climatic, eustatic and genomic data. Consequently, we point out that the P-Tr extinction was caused by the tectonically originated climate instability. We also clarify that the overall trend of biodiversification originated from the underlying genome size evolution, and that the fluctuation of biodiversity originated from the interactions among the earth's spheres. The evolution at molecular level had played a significant role for the survival of life from environmental disasters.

RESULTS

Let us go back to the early history of our planet, and gaze at these just originated lives. They seemed so delicate, however they were indeed persistent and dauntless. They had a lofty aspiration to live on until the end of the earth; otherwise the rare opportunity of this habitable planet in the wildness of space may be wasted. Their story continued and was recorded in the big book of stratum. This story was so magnificent that we were moved to tears time and again. Was the life just lucky to survive from all the disasters, or innately able to contend with any possible challenges in the environment? Before answering this question, we should explain the evolution of biodiversity by appropriate driving forces.

Again, let us go back to mid nineteenth century, and size up the situations for the founders of evolutionism. They were completely unaware of the molecular evolution; they knew little about the marine regression or transgression and paleoclimate; and they possessed poor fossil records. However, they still pointed out the right direction to understand the evolution of life by their keen insight. What is the mission then for contemporary evolutionists in floods of genomic and stratum data? Can we go a little further than endless debates?

The Sepkoski curve based on fossil records indicates the Phanerozoic biodiversity evolution [1] [2] [3], where we can observe five mass extinctions, the background extinction, and its increasing overall trend. The main purpose of this paper is to explain the Sepkoski curve by a tectono-genomic curve based on climatic, eustatic (sea level) and genomic data. We propose a split scenario to study the biodiversity evolution at the species level and at the molecular level separately. We construct a tectonic curve based on climatic and eustatic data to explain the fluctuations in the Sepkoski curve. And we also construct a genomic curve based on genomic data to explain the overall trend of the Sepkoski curve. Thus, we obtain a tectono-genomic curve by synthesizing the tectonic curve and the genomic curve, which agrees with the Sepkoski curve not only in overall trend but also in detailed fluctuations (Fig 1):

$$Curve_Sepkoski \approx Curve_TectonoGenomic.$$

We observe that both the tectono-genomic curve and the Sepkoski curve decline at each time of

the five mass extinctions (O-S, F-F, P-Tr, Tr-J and K-Pg). The growth rates of the tectono-genomic curve and the Sepkoski curve also coincide with each other. Hence, we show that the biodiversity evolution is driven by both the tectonic movement and the genome size evolution. The main steps in constructing the tectono-genomic curve are as follows.

(1) We obtained the consensus climate curve (*Curve_CC*), the consensus sea level curve (*Curve_SL*) and the biodiversification curve (*Curve_BD*) to describe the Phanerozoic climate change, sea level fluctuation and biodiversity variation respectively (Fig 2a). (i) We obtained *Curve_CC* by synthesizing the following three independent results on Phanerozoic climate change in a pragmatic approach (Fig S1a): Berner’s atmosphere CO_2 curve [4], the Phanerozoic global climatic gradients revealed by climatically sensitive sediments [5] [6], and the Phanerozoic $^{87}Sr/^{86}Sr$ curve [7]; (ii) We obtained *Curve_SL* by synthesizing the result in ref. [8] and the results in ref. [9] [10] (Fig. S1c); and (iii) We obtained *Curve_BD* based on fossil record (Fig. 2d).

(2) We calculated the correlation coefficients $r_{\mu\nu}^o$ among *Curve_CC*, *Curve_SL* and *Curve_BD* (Table 1). The correlation coefficient between *Curve_BD* and *Curve_SL* in the Phanerozoic eon is $r_{SB}^{PMC} = 0.564$, which generally indicates a same phase between *Curve_BD* and *Curve_SL*. The correlation coefficients between *Curve_BD* and *Curve_CC*, and between *Curve_SL* and *Curve_CC* in the Paleozoic era are $r_{BC}^P = 0.114 > 0$ and $r_{CS}^P = 0.494 > 0$ respectively, which generally indicate the same variation pattern (or the same phase) of *Curve_CC* with *Curve_BD* and *Curve_SL* in the Paleozoic era. While the correlation coefficients between *Curve_BD* and *Curve_CC*, and between *Curve_SL* and *Curve_CC* in the Mesozoic era are $r_{BC}^M = -0.431 < 0$ and $r_{CS}^M = -0.617 < 0$ respectively, which indicate a “climate phase reverse event” from same phase to opposite phase in P-Tr boundary. In the supplementary methods, we confirm the reality of such a “climate phase reverse event” by verifications for 10 group curves based on candidate climate, biodiversity and sea level data. Therefore, when constructing the tectonic curve based on *Curve_SL* and *Curve_CC*, we chose a positive sign for *Curve_SL* throughout the Phanerozoic eon; and we chose a positive sign for *Curve_CC* only in the Paleozoic era, but a negative sign for *Curve_CC* in the Mesozoic and Cenozoic eras (Fig S1e).

(3) The overall trend in biodiversity evolution is about an exponential function [11]: $N_{genus} = N_{genus}^0 \exp(-t/\tau_{BD})$. Based on the relationship between certain average genome sizes in taxa and their origin time, we found that the overall trend in genome size evolution is also an exponential function [12] [13] (Fig 3a): $N_{genome} = N_{genome}^0 \exp(-t/\tau_{GS})$. The log-normal genome size distributions (Fig S2a, 3b) and the exponential asymptotes of the accumulation origination and extinction number of genera (Fig 2d) also indicate the exponential growth trend in genome size evolution. We found that the “e-folding” time of the biodiversity evolution $\tau_{BD} = 259.08$ Million years (Myr) is approximately equal to the “e-folding” time of the genome size evolution $\tau_{GS} = 256.56$ Myr (Fig 3d):

$$\tau_{BD} \approx \tau_{GS}.$$

Hence, we can explain the overall trend in biodiversity evolution by constructing the genomic curve based on τ_{GS} .

In the split scenario, we can explain the declining Phanerozoic background extinction rates [14] [15] according to the equation:

$$rate_{o+e} = \exp(-k_{GS} \cdot (-t + 542.0)) \cdot rate_{essential},$$

where the declining factor $\exp(-k_{GS} \cdot (-t + 542.0))$ is due to the increasing overall trend in genome size evolution (Fig 2c). The underlying genomic contribution to the biodiversity evolution prevents the life from being completely wiped out by uncertain disasters.

So far, we have explained the declining background extinction rates and the increasing overall trend of the Sepkoski curve. The remaining problem is to explain the mass extinctions. Since we have successfully fulfilled the tectono-genomic curve to explain the Sepkoski curve, the reasons that caused the fluctuations in the tectono-genomic curve are just what caused the mass extinctions. We should emphasize here that the fluctuations in the tectono-genomic curve have nothing to do with the fossil data. According to the methods in constructing the tectono-genomic curve, we conclude that the mass extinctions were caused by both the sea level fluctuations and the climate changes. We refer it as the tectonic cause of the mass extinctions, which rules out any celestial explanations.

Furthermore, we point out that the greatest P-Tr extinction uniquely involved the climate phase reverse event, which occurred not just coincidentally with the formation of Pangaea and the atmosphere composition variation [4] [16] [17]. The fossil record indicates a two-stage pattern at the Guadalupian-Lopingian boundary (GLB) [18] [19] [20] and at the Permian-Triassic Boundary (PTB) [21] [22]. In detail, it also indicates a multi-episode pattern in the PTB stage [23] [24]. The P-Tr mass extinction was by no means just one single event. The multi-stage/episode pattern can hardly be explained by the large igneous province event [25] [26]. We can explain the above two stages by two sharp peaks observed in d_{CC} (the variation rate curve of *Curve_CC*) at GLB and PTB respectively, which show that the temperature increased extremely rapidly at GLB and decreased extremely rapidly at PTB (Fig 2b). The different climate at GLB and at PTB resulted in different extinction time for Fusulinina (at GLB) and Endothyridina (at PTB).

At last, we will focus on the genomic contribution to the biodiversity evolution. We can obtain both the phylogenetic tree of species (Fig S3a, 4c by M_{ci}) and the evolutionary tree of 64 codons (Fig 4a, S3b by M_{codon}) based on the same codon interval correlation matrix Δ . This is a direct evidence to show the close relationship between the molecular evolution and the biodiversity evolution. On one hand, the result is reasonable in obtaining the tree of species. This universal phylogenetic method based on M_{ci} applies for Bacteria, Archaea, Eukarya and virus. On the other hand, the result is valid in understanding the genetic code evolution [27] [28] [29]. And an average codon distance curve *Barrier* based on M_{codon} reveals a midway “barrier” in the genetic code evolution (Fig 4b, S3c). Moreover, we can testify the three-stage pattern (Basal metazoa, Protostomia and Deuterostomia) in Metazoan origination [30] according to the genome size evolution. Favorable phylogenetic trees can also be obtained by the correlation matrices M_{gs} based on genome size data (Fig 3c, S2c, S2d).

METHODS

1 Data resources and notations

1.1 Data resources

- (1) Phanerozoic climate change data: ref. [4], [5], [6], [7];
- (2) Phanerozoic sea level fluctuation data: ref. [8], [9], [10];
- (3) Phanerozoic biodiversity variation based on fossil records: ref. [1], [2], [3];
- (4) Genome size databases: Animal Genome Size Database [31], Plant DNA C-values Database [32];
- (5) Whole genome database: GenBank.

1.2 Notations

Sepkoski curve	:	$Curve_Sepkoski$	
tecontogenomic curve	:	$Curve_TectonoGenomic$	
time	:	t, T	
biodiversity curves	:	$Curve_BD, BD, Total-BD$	
sea level curves	:	$Curve_SL, S^1, S^2, S_w$	
climate curves	:	$Curve_CC, C^1, C^2, C^3, C_{w1}, C_{w2}, C_w$	
correlation coefficients	:	$r_{\mu\nu}^\rho, R^+, R^-, \Delta R, Q, Q', \Delta Q$	
climate phases	:	$CPI, CPII, CPIII$	
genome sizes	:	$G, G_{sp}, G_{mean_log}, G_{sd_log}, G^*$	(1)
biodiversity variation rates	:	$rate_ori, rate_ext, rate_essential$	
derivative curves	:	d_CC, d_SL, d_BD	
overall trends	:	$OT-BD, OT-GS$	
e-folding times and growth rates	:	$\tau_{BD}, k_{BD}, \tau_{GS}, k_{GS}$	
genomes size distributions and matrices	:	D_{gs}, M_{gs}	
codon interval distributions and matrices	:	$D_{ci}, \Delta, M_{ci}, M_{codon}$	
genetic code evolutionary curves	:	$Barrier, Hurdle.$	

1.3 Math notations

Let $sum(V)$, $mean(V)$, $std(V)$, $log(V)$ and $exp(V)$ denote respectively the summation, mean, stand deviation, logarithm and exponent of a vector $V(i)$, $i = 1, 2, \dots, i_m$:

$$sum(V) = \sum_{i=1}^{i_m} V(i) \quad (2)$$

$$mean(V) = \frac{1}{i_m} sum(V) \quad (3)$$

$$std(V) = \sqrt{mean((V - mean(V))^2)} \quad (4)$$

$$log(V) = [\log_e(V(1)), \log_e(V(2)), \dots, \log_e(V(i_m))] \quad (5)$$

$$exp(V) = [\exp(V(1)), \exp(V(2)), \dots, \exp(V(i_m))]. \quad (6)$$

Especially, let $nondim(V)$ denote the operation of nondimensionalization for a dimensional vector V ,

$$nondim(V) = (V - mean(V))/std(V). \quad (7)$$

In this paper, we obtain respectively the dimensionless vectors $Curve_BD$, $Curve_CC$, $Curve_SL$, etc. after nondimensionalization based on the dimensional raw data of biodiversity curve, climate curve and sea level curve in the Phanerozoic eon.

Let $corrcoef(V, U)$, $max(V, U)$, $min(V, U)$ and $[V, U]$ denote respectively the correlation coefficient, maximum and minimum of a pair of vectors $V(i)$ and $U(i)$ ($i = 1, 2, \dots, i_m$):

$$corrcoef(V, U) = \frac{\sum_{i=1}^{i_m} (V(i) - mean(V))(U(i) - mean(U))}{\sqrt{\sum_{i=1}^{i_m} (V(i) - mean(V))^2} \sqrt{\sum_{i=1}^{i_m} (U(i) - mean(U))^2}} \quad (8)$$

$$max(V, U) = [max(V(1), U(1)), max(V(2), U(2)), \dots, max(V(i_m), U(i_m))] \quad (9)$$

$$min(V, U) = [min(V(1), U(1)), min(V(2), U(2)), \dots, min(V(i_m), U(i_m))]. \quad (10)$$

Let $\frac{d}{dt}(V)$ denote the discrete derivative of $V(t)$ with respect to time t :

$$\frac{d}{dt}(V) = [\frac{dV}{dt}|_{t=t(1)}, \dots, \frac{dV}{dt}|_{t=t(i_m)}], \quad (11)$$

where $V(t) = [V(1), V(2), \dots, V(i_m)]$ is an i_m -element discrete function of time $t = [t(1), t(2), \dots, t(i_m)]$. The linear interpolation of V is denoted by:

$$[V(1), V(2), \dots, V(i'_m)] = \text{interp}([t(1), \dots, t(i_m)], [V(1), \dots, V(i_m)], [t(1), \dots, t(i'_m)]). \quad (12)$$

The concatenation of function $V(t)$ between period $t([P_1]) = [t(i_1), t(i_1 + 1), \dots, t(i_2)]$ and period $t([P_2]) = [t(i_2 + 1), t(i_2 + 2), \dots, t(i_3)]$ is denoted by:

$$[V([P_1]), V([P_2])] = [V(i_1), \dots, V(i_2), V(i_2 + 1), \dots, V(i_3)], \quad (13)$$

where $P_1 = [i_1, i_1 + 1, \dots, i_2]$ and $P_2 = [i_2 + 1, i_2 + 2, \dots, i_3]$ are parts of the indices. For a i_m -by- j_m array $M(i, j)$, let $M(i, :)$ denote

$$M(i, :) = [M(i, 1), M(i, 2), \dots, M(i, j_m)]. \quad (14)$$

2 Understanding the Sepkoski curve through the tectono-genomic curve

The Phanerozoic biodiversity curve has been explained in this paper. We propose a split scenario for the biodiversity evolution:

$$\text{Biodiversity evolution} = \text{Tectonic contribution} + \text{Genomic contribution}. \quad (15)$$

We construct a tectono-genomic curve based on climatic, eustatic (sea level) and genomic data, which agrees with the Phanerozoic biodiversity curve based on fossil records very well. We explain the P-Tr extinction by a climate phase reverse event. And we point out that the biodiversity evolution was driven independently at the species level as well as at the molecular level.

3 The overall trend of biodiversity evolution

3.1 Motivation

A split scenario is propose to separate the Phanerozoic biodiversity evolution curve into its exponential growth part and its variation part.

3.2 The exponential outline of the Sepkoski curve

The Phanerozoic biodiversity curve (namely the Sepkoski curve) can be obtained based on fossil records. We denote the Phanerozoic genus number biodiversity curve in ref. [2] after linear interpolation by (Fig 1):

$$Curve_Sepkoski(t) : \text{ref. [2]}, \quad (16)$$

which is a 5421-element function of time t , from 542 million years ago (Ma) to 0 Ma in step of 0.1 million of years (Myr):

$$\begin{aligned} t &= [t(1), t(2), t(3), \dots, t(5419), t(5420), t(5421)] \\ &= [542.0, 541.9, 541.8, \dots, 0.2, 0.1, 0]. \end{aligned} \quad (17)$$

The outline of $Curve_Sepkoski(t)$ is an exponential function:

$$N_{genus}(t) = N_{genus}^0 \exp(-t/\tau_{BD}), \quad (18)$$

where the genera number constant is $N_{genus}^0 = 2690$ genera, and the “e-folding time” of the biodiversity evolution is $\tau_{BD} = 259.08$ Myr.

3.3 The split scenario of the Sepkoski curve

We define the total biodiversity curve $Total-BD$ in the Phanerozoic eon by the logarithm of $Curve_Sepkoski$:

$$Total-BD = \log(Curve_Sepkoski(t)), \quad (19)$$

which is also a 5421-element function of time t . According to the linear regression analysis, the regression line of $Total-BD$ on t is defined as the overall trend of total biodiversity curve:

$$\begin{aligned} OT-BD &= \log(N_{genus}(t)) \\ &= k_{BD} \cdot (-t) + \log(N_{genus}^0), \end{aligned} \quad (20)$$

where the growth rate of biodiversity evolution, namely the slope of this regression line, is $k_{BD} = 1/\tau_{BD} = 0.0038598 \text{ Myr}^{-1}$.

We propose a “split scenario” in observing the Phanerozoic biodiversity evolution by separating the Sepkoski curve into its exponential growth part and its variation part. In this scenario, the total

biodiversity curve $Total-BD$ can be written as the summation of its linear part $OT-BD$ and its net variation part BD (Fig. 2d):

$$Total-BD = OT-BD + BD. \quad (21)$$

Hence, we obtain the biodiversity curve $Curve_BD$ after nondimensionalization of BD :

$$Curve_BD = nondim(BD). \quad (22)$$

4 The tectonic cause of mass extinctions

4.1 Motivation

We construct the tectonic curve based on the climatic and eustatic data in consideration of the phase relationships among $Curve_BD$, $Curve_CC$ and $Curve_SL$.

4.2 The consensus climate curve

We denote the three independent results on Phanerozoic global climate in ref. [5] [6], [7], [4] as C_0^1 , C_0^2 , C_0^3 respectively after linear interpolation:

$$C_0^1(t) : \text{ref. [5] [6]}, \quad (23)$$

$$C_0^2(t) : \text{ref. [7]}, \quad (24)$$

$$C_0^3(t) : \text{ref. [4]}. \quad (25)$$

The missing $^{87}Sr/^{86}Sr$ in ref. [7] in lower Cambrian are obtained from ref. [33] for C_0^2 . We obtain three dimensionless global climate curves after nondimensionalization:

$$C^1(t) = nondim(C_0^1(t)), \quad (26)$$

$$C^2(t) = nondim(C_0^2(t)), \quad (27)$$

$$C^3(t) = nondim(C_0^3(t)). \quad (28)$$

Hence, we obtain the consensus climate curve $Curve_CC$ by synthesizing the above three results C^1 , C^2 and C^3 (Fig. S1a):

$$Curve_CC = nondim((C^1 + C^2 + C^3)/3). \quad (29)$$

4.3 The consensus sea level curve

We denote the Phanerozoic sea level curves in ref. [8] and in ref. [9] [10] as S_0^1 and S_0^2 (via linear interpolation) respectively:

$$S_0^1(t) : \text{ref. [8]}, \quad (30)$$

$$S_0^2(t) : \text{ref. [9] [10]}. \quad (31)$$

And we obtain the dimensionless sea level curves after nondimensionalization:

$$S^1(t) = nondim(S_0^1(t)), \quad (32)$$

$$S^2(t) = nondim(S_0^2(t)). \quad (33)$$

Hence we obtain the consensus sea level curve $Curve_SL$ by synthesizing the two results S^1 and S^2 (Fig. S1c):

$$Curve_SL = nondim((S^1 + S^2)/2). \quad (34)$$

We can obtain the derivative curves d_CC , d_SL and d_BD respectively as follows (Fig. 2b):

$$d_CC = \frac{d}{dt}(Curve_CC) \quad (35)$$

$$d_SL = \frac{d}{dt}(Curve_SL) \quad (36)$$

$$d_BD = \frac{d}{dt}(Curve_BD). \quad (37)$$

4.4 Correlation coefficients among $Curve_CC$, $Curve_SL$ and $Curve_BD$

So far, we have obtained the first group ($n = 1$) of curves $Curve_CC$, $Curve_SL$ and $Curve_BD$ to describe the Phanerozoic climate, sea level and biodiversity. They are all 5421-element functions of time t .

There are three eras (Paleozoic, Mesozoic and Cenozoic) in the Phanerozoic eon, the time t in the Phanerozoic eon can be concatenated as follow:

$$t = [t([P]), t([M]), t([C])], \quad (38)$$

where the indices for the Paleozoic, Mesozoic and Cenozoic are as follows respectively:

$$P = [(5421 - 5420), \dots, (5421 - 2510)], \text{ for Paleozoic from 542.0 Ma to 251.0 Ma,} \quad (39)$$

$$M = [(5421 - 2510 + 1), \dots, (5421 - 655)], \text{ for Mesozoic from 251.0 Ma to 65.5 Ma,} \quad (40)$$

$$C = [(5421 - 655 + 1), \dots, 5421], \text{ for Cenozoic from 65.5 Ma to today.} \quad (41)$$

Similarly, we define the indices for the other periods as follows:

$$PMC : \text{ for Phanerozoic from 542.0 Ma to 0 Ma,} \quad (42)$$

$$PM : \text{ for Paleozoic and Mesozoic from 542.0 Ma to 65.5 Ma,} \quad (43)$$

$$MC : \text{ for Mesozoic and Cenozoic from 251.0 Ma to 0 Ma,} \quad (44)$$

$$P \setminus L : \text{ for Paleozoic except for Lopingian from 542.0 Ma to 260.4 Ma,} \quad (45)$$

$$L : \text{ for Lopingian from 260.4 Ma to 251.0 Ma,} \quad (46)$$

$$L.M.Tr : \text{ for Lower and Middle Triassic from 251.0 Ma to 228.7 Ma,} \quad (47)$$

$$M \setminus L.M.Tr : \text{ for Mesozoic except for Lower and Middle Triassic from 228.7 Ma to 65.5 Ma.} \quad (48)$$

We can calculate the correlation coefficients $r_{\mu\nu}^\rho$ among $Curve_CC$, $Curve_SL$ and $Curve_BD$ in certain periods respectively (Data.2):

$$r_{\mu\nu}^\rho = corrcoeff(\text{curve } \mu([\rho]), \text{curve } \nu([\rho])) \quad (49)$$

where the subscripts

$$\mu, \nu = C, S, B \quad (50)$$

for the curves $Curve_CC$, $Curve_SL$ and $Curve_BD$ respectively, and the superscript

$$\rho = P, M, C, PMC, PM, MC, P \setminus L, L, L.M.Tr, M \setminus L.M.Tr \quad (51)$$

for the corresponding periods respectively.

Note: The correlation coefficients generally agree with one other in the calculations between *Curve_BD* and any of *Curve_SL*, S^1 , S^2 , or between *Curve_BD* and any of *Curve_CC*, C^1 , C^2 , C^3 , i.e. in general:

$$r_{\mu\nu}^{\rho}(n) \sim r_{\mu\nu}^{\rho}(n'), \quad n, n' = 1, 2, \dots, 10. \quad (52)$$

Therefore, the phase relationship of *Curve_CC*, *Curve_SL* and *Curve_BD* is generally irrelevant with the weights in obtaining *Curve_CC* and *Curve_SL*. The correlation coefficients are also irrelevant whether we nondimensionalize the curves, for instance:

$$\begin{aligned} & \text{corrcoef}((S^1([P]) + S^2([P]))/2, BD([P])) \\ = & \text{corrcoef}(\text{nondim}((S^1([P]) + S^2([P]))/2), \text{nondim}(BD([P]))) \\ = & \text{corrcoef}(\text{Curve_SL}([P]), \text{Curve_BD}([P])) \\ = & r_{SB}^P. \end{aligned} \quad (53)$$

Note: The first group ($n = 1$) of curves *Curve_CC*, *Curve_SL* and *Curve_BD* is the best among the 10 similar groups of curves to describe the Phanerozoic climate, sea level and biodiversity.

4.5 Three climate phases

We propose three climate patterns CP I, CP II and CP III in the Phanerozoic eon based on the positive or negative correlations among *Curve_CC*, *Curve_SL* and *Curve_BD*. Interestingly, the time between the positive correlation periods and the negative correlation periods agree with the Paleozoic-Mesozoic boundary and the Mesozoic-Cenozoic boundary.

(1) We have

$$r_{SB}^P = 0.5929 > 0 \quad (54)$$

$$r_{BC}^P = 0.1136 > 0 \quad (55)$$

$$r_{CS}^P = 0.4942 > 0 \quad (56)$$

which indicate the positive correlations among *Curve_CC*, *Curve_SL* and *Curve_BD* in the Paleozoic era. This is called the first climate pattern (CP I);

(2) We have

$$r_{SB}^M = 0.9054 > 0 \quad (57)$$

$$r_{BC}^M = -0.4308 < 0 \quad (58)$$

$$r_{CS}^M = -0.6171 < 0 \quad (59)$$

which indicate the negative correlations between *Curve_CC* and *Curve_SL* and between *Curve_CC* and *Curve_BD*, and the positive correlation between *Curve_SL* and *Curve_BD* in the Mesozoic era. This is called the second climate pattern (CP II);

(3) We have

$$r_{SB}^C = -0.8314 < 0 \quad (60)$$

$$r_{BC}^C = -0.8814 < 0 \quad (61)$$

$$r_{CS}^C = 0.9501 > 0 \quad (62)$$

which indicate the negative correlations between *Curve_CC* and *Curve_BD* and between *Curve_SL* and *Curve_BD*, and the positive correlation between *Curve_SL* and *Curve_CC* in the Cenozoic era. This is called the third climate pattern (CP III).

We define the average correlation coefficient R^+ in the positive correlation periods:

$$R^+ = \frac{w^P \cdot r_{SB}^P + w^P \cdot r_{BC}^P + w^P \cdot r_{CS}^P + w^M \cdot r_{SB}^M + w^C \cdot r_{CS}^C}{w^P + w^P + w^P + w^M + w^C}, \quad (63)$$

and the average correlation coefficient R^- in the negative correlation periods:

$$R^- = \frac{w^M \cdot r_{BC}^M + w^M \cdot r_{CS}^M + w^C \cdot r_{SB}^C + w^C \cdot r_{BC}^C}{w^M + w^M + w^C + w^C}, \quad (64)$$

where the weights w^p are the durations of Paleozoic, Mesozoic and Cenozoic respectively:

$$w^P = 542.0 - 251.0 = 291.0 \text{ Myr} \quad (65)$$

$$w^M = 251.0 - 65.5 = 185.5 \text{ Myr} \quad (66)$$

$$w^C = 65.5 \text{ Myr}. \quad (67)$$

And we denote the difference between R^+ and R^- as

$$\Delta R = R^+ - R^-. \quad (68)$$

We define the average abstract correlation coefficient Q for the positive as well as the negative correlation periods as:

$$Q = \frac{1}{w^P + w^M + w^C} \sum_{\rho=P,M,C} w^\rho \cdot (|r_{SB}^\rho| + |r_{BC}^\rho| + |r_{CS}^\rho|), \quad (69)$$

and the average abstract correlation coefficient Q' for the mixtures of positive and negative correlation periods as:

$$Q' = \frac{1}{w^{PMC} + w^{PM} + w^{MC}} \sum_{\rho=PMC,PM,MC} w^\rho \cdot (|r_{SB}^\rho| + |r_{BC}^\rho| + |r_{CS}^\rho|), \quad (70)$$

where the remaining weights w^ρ are:

$$w^{PMC} = 542.0 \text{ Myr} \quad (71)$$

$$w^{PM} = 542.0 - 65.5 = 476.5 \text{ Myr} \quad (72)$$

$$w^{MC} = 251.0 \text{ Myr}. \quad (73)$$

And we denote the difference between Q and Q' as

$$\Delta Q = Q - Q'. \quad (74)$$

We found that the abstract correlation coefficients $|r_{\mu\nu}^{PMC}|$, $|r_{\mu\nu}^{PM}|$ and $|r_{\mu\nu}^{MC}|$ in the mixtures of positive and negative periods $\rho = PMC, PM, MC$ are obviously less than the abstract values $|r_{\mu\nu}^P|$, $|r_{\mu\nu}^M|$ and $|r_{\mu\nu}^C|$ in the positive or negative periods, namely in the Paleozoic, Mesozoic and Cenozoic eras. Therefore, the three climate patterns naturally correspond to the Paleozoic, Mesozoic and Cenozoic eras respectively. Based on the data of the first group (n=1) of curves *Curve_CC*, *Curve_SL* and *Curve_BD*, we have:

$$R^+ = R^+(1) > 0 \text{ (tend to be equal to 1)} \quad (75)$$

$$R^- = R^-(1) < 0 \text{ (tend to be equal to -1)} \quad (76)$$

$$\Delta R = \Delta R(1) \gg 0 \quad (77)$$

$$Q = Q(1) \sim 1 \text{ (tend to be equal to 1)} \quad (78)$$

$$Q' = Q'(1) \sim 0 \text{ (tend to be equal to 0)} \quad (79)$$

$$\Delta Q = \Delta Q(1) > 0 \quad (80)$$

which furthermore shows that the division of three climate patterns CP I, CP II and CP III is essential property of the evolutionary earth's spheres.

Note: These relations are still valid for the other groups of curves ($n = 2, 3, \dots, 10$).

4.6 The P-Tr extinction was caused by the climate phase reverse between CP I and CP II

We summarize the reasons to explain the P-Tr extinction by the climate phase reverse event as follows.

- Successful explanation of the Sepkoski curve by the tectono-genomic curve based on the climate phase reverse event (Fig 1)
- The climate phase reverse event between CP I and CP II happened at P-Tr boundary (Fig 2a)
- The sharp peaks of d_{CC} at the Guadalupian-Lopingian boundary and at the P-Tr boundary (Fig 2b)
- Abnormal climate trend in the Lopingian epoch
- Different animal extinction patterns at the Guadalupian-Lopingian boundary and at the P-Tr boundary.

4.7 The tectonic curve and the tectonic contribution to the biodiversity variation

The phase of *Curve_{SL}* is about the same with the phase of *Curve_{BD}* in the Phanerozoic eon. And the phase of *Curve_{CC}* is about the same with the phase of *Curve_{BD}* in the Paleozoic era (CP I), while it is about the opposite in the Mesozoic era (CP II) and in the Cenozoic era (CP III). Accordingly, we define the associate tectonic curve *Curve_{Tectonic_0}* by combining the consensus

sea level curve and the consensus climate curve as follow (Fig S1e):

$$\begin{aligned} Curve_Tectonic_0 = & [(Curve_SL([P]) + Curve_CC([P]))/2, \\ & (Curve_SL([MC]) - Curve_CC([MC]))/2]. \end{aligned} \quad (81)$$

We define the tectonic curve $Curve_Tectonic$ with the same standard deviation of the net variation biodiversity curve BD :

$$Curve_Tectonic = (Curve_Tectonic_0 - mean(Curve_Tectonic_0)) \cdot a_{std}, \quad (82)$$

where

$$a_{std} = \frac{std(BD)}{std(Curve_Tectonic_0 - mean(Curve_Tectonic_0))}. \quad (83)$$

The tectonic curve $Curve_Tectonic$ represents the tectonic (sea level and climate) contribution to the biodiversity evolution. We can calculate the correlation coefficient between the tectonic curve and the biodiversity curve in the Paleozoic era or in the Mesozoic and Cenozoic eras:

$$\begin{aligned} r_{B+}^P &= corrcoeff(Curve_Tectonic([P]), Curve_BD([P])) \\ &= 0.421, \end{aligned} \quad (84)$$

$$\begin{aligned} r_{B-}^{MC} &= corrcoeff(Curve_Tectonic([MC]), Curve_BD([MC])) \\ &= 0.878. \end{aligned} \quad (85)$$

Accordingly, we found that the tectonic curve $Curve_Tectonic$ is positively correlated with the biodiversity curve $Curve_BD$ either in the Paleozoic era or in the Mesozoic and Cenozoic eras.

5 The genomic contribution to the biodiversity evolution

5.1 Motivation

We construct the genomic curve based on the observation of equality between the growth rate k_{GS} in genome size evolution and the growth rate k_{BD} in biodiversity evolution.

5.2 The overall trend of genome size evolution

5.2.1 The log-normal distribution of genome size

We found that the genome sizes of species in a taxon are log-normally distributed in general, which were verified in the following 7 taxa (Fig. S2a):

$$\log(G(\lambda, sp(\lambda))) \text{ are normally distributed,} \quad (86)$$

where $G(\lambda, sp(\lambda))$ are the genome sizes of all the species $sp(\lambda)$ ($sp(\lambda) = 1, 2, \dots, s_m(\lambda)$) in the taxon λ in the genome size databases, and

$$\begin{aligned} \lambda = 1 & : \text{Diploblostica} \\ \lambda = 2 & : \text{Protostomia} \\ \lambda = 3 & : \text{Deuterostomia} \\ \lambda = 4 & : \text{Bryophyte} \\ \lambda = 5 & : \text{Pteridophyte} \\ \lambda = 6 & : \text{Gymnosperm} \\ \lambda = 7 & : \text{Angiosperm.} \end{aligned} \quad (87)$$

Due to the additivity of normal distribution, the genome sizes of animals, plants, or eukaryotes are also log-normal distributed. We obtain the means of logarithm of genome sizes and the standard deviations of logarithm of genome sizes as follows:

$$G_{mean_log}^P(\lambda) = \text{mean}(\log(G(\lambda, sp(\lambda)))), \quad (88)$$

and

$$G_{sd_log}^P(\lambda) = \text{std}(\log(G(\lambda, sp(\lambda)))), \quad (89)$$

where $sp(\lambda) = 1, 2, \dots, s_m(\lambda)$. Denote G^* as the mean logarithm of genome sizes of all the contemporary eukaryotes:

$$G^* = \text{mean}(\log(G(sp))), \quad (90)$$

where sp is all the contemporary eukaryotes in the genome size databases.

Note: The log-normal distribution of genome size can be demonstrated by the common intersection point Ω for the following regression lines (Fig 3b):

$$\text{regression line of } G_{mean_log}(\lambda') \text{ on } G_{sp}(\lambda') \quad (91)$$

$$\text{regression line of } G_{\text{mean_log}}(\lambda') \pm \chi \cdot G_{\text{sd_log}}(\lambda') \text{ on } G_{\text{sp}}(\lambda') \quad (92)$$

$$\text{regression line of } G_{\text{mean_log}}(\lambda') \pm \chi' \cdot G_{\text{sd_log}}(\lambda') \text{ on } G_{\text{sp}}(\lambda') \quad (93)$$

$$\text{regression line of } \max(G(\lambda', \text{sp}(\lambda'))) \text{ on } G_{\text{sp}}(\lambda') \quad (94)$$

$$\text{regression line of } \min(G(\lambda', \text{sp}(\lambda'))) \text{ on } G_{\text{sp}}(\lambda') \quad (95)$$

$$\text{regression line of } G_{\text{mean_log}}^P(\lambda) \text{ on } G_{\text{sp}}^P(\lambda) \quad (96)$$

$$\text{regression line of } G_{\text{mean_log}}^P(\lambda) \pm \chi \cdot G_{\text{sd_log}}^P(\lambda) \text{ on } G_{\text{sp}}^P(\lambda) \quad (97)$$

$$\text{regression line of } G_{\text{mean_log}}^P(\lambda) \pm \chi' \cdot G_{\text{sd_log}}^P(\lambda) \text{ on } G_{\text{sp}}^P(\lambda) \quad (98)$$

$$\text{regression line of } \max(G(\lambda, \text{sp}(\lambda))) \text{ on } G_{\text{sp}}^P(\lambda) \quad (99)$$

$$\text{regression line of } \min(G(\lambda, \text{sp}(\lambda))) \text{ on } G_{\text{sp}}^P(\lambda) \quad (100)$$

where $\lambda = 1, 2, \dots, 7$ for the above 7 taxa, $\lambda' = 1, 2, \dots, 19+53$ for 19 animal taxa and 53 angiosperm taxa, $\chi = 1.5677$ and $\chi_1 = 3.1867$. The values of $G_{\text{sd_log}}$ tend to decline with respect to G_{sp} that is proportional to the origin time of taxa (Fig S2b).

5.2.2 The exponential overall trend of genome size evolution

We assume the approximate origin times $T(\lambda)$ for the taxa $\lambda = 1, 2, \dots, 7$ as follows:

$$\begin{aligned} T(1) &= 560.0 \text{ Ma} \\ T(2) &= 542.0 \text{ Ma, PreCm-Cm} \\ T(3) &= 525.0 \text{ Ma} \\ T(4) &= 488.3 \text{ Ma, Cm-O} \\ T(5) &= 416.0 \text{ Ma, S-D} \\ T(6) &= 359.2 \text{ Ma, D-C} \\ T(7) &= 145.5 \text{ Ma, J-K} \end{aligned} \quad (101)$$

We observed a rough proportional relationship between $G_{\text{mean_log}}^P(\lambda)$ and $T(\lambda)$. Because $G_{\text{mean_log}}^P(\lambda)$ is the mean genome size of the “contemporary species”, we should introduce a new notion (the specific genome size) to indicate the mean genome sizes of the “ancient species” in taxa $\lambda = 1, 2, \dots, 7$ at its origin time $T(\lambda)$. Here, we define the specific genome size G_{sp}^P as:

$$G_{\text{sp}}^P(\lambda) = G_{\text{mean_log}}^P(\lambda) - \chi \cdot G_{\text{sd_log}}^P(\lambda), \quad (102)$$

where we let $\chi = 1.5677$ such that the intercept of the regression line of $G_{\text{sp}}^P(\lambda)$ on $T(\lambda)$ is equal to G^* . We found that $G_{\text{sp}}^P(\lambda)$ is generally proportional to $T(\lambda)$ (Fig. 3a). We define the regression line

of $G_{sp}^P(\lambda)$ on $T(\lambda)$ as overall trend of genome size curve:

$$OT-GS = k_{GS}(-t) + \log(N_{genome}^0). \quad (103)$$

This equation is equivalent to the exponential overall trend of genome size evolution:

$$N_{genome}(t) = N_{genome}^0 \exp(-t/\tau_{GS}), \quad (104)$$

where the genome size constant is $N_{genome}^0 = 2.16 \times 10^9$ base pairs (bp) and the “e-folding time” in genome size evolution is $\tau_{GS} = 256.56$ (Myr). The growth rate (namely the slope) of $OT-GS$ is $k_{GS} = 1/\tau_{GS} = 0.0038977 \text{ Myr}^{-1}$.

Note: The exponential overall trend of genome size evolution obtained in the Phanerozoic eon can be extrapolated to the Precambrian period. This extrapolation result according to the value of k_{GS} is reasonable to show that the least genome size at 3800 Ma (about the beginning of life) is about several hundreds of base pairs (Fig 3d).

5.3 The agreement between the overall trend of genome size evolution and the overall trend of biodiversity evolution

We found the closely relationship between the genome size evolution and the biodiversity evolution (Fig 3d). Both the overall trend of genome size evolution and the overall trend of biodiversity evolution are exponential; and the exponential growth rate in the genome size evolution ($k_{GS} = 0.0038977 \text{ Myr}^{-1}$) (Fig 3a, 3d) is approximately equal to the exponential growth rate in the biodiversity evolution ($k_{BD} = 0.0038598 \text{ Myr}^{-1}$) (Fig 2d, 3d):

$$k_{GS} \approx k_{BD}, \quad (105)$$

which is equivalent to that the e-folding time in the genome size evolution ($\tau_{GS} = 256.56 \text{ Myr}$) is approximately equal to the e-folding time in the biodiversity evolution ($\tau_{BD} = 259.08 \text{ Myr}$):

$$\tau_{GS} \approx \tau_{BD}. \quad (106)$$

5.4 Explanation of the declining Phanerozoic background extinction rates

Let $rate_ori$ and $rate_ext$ denote the Phanerozoic biodiversity origination rate and extinction rate respectively:

$$rate_ori : \text{ref. [2]}, \quad (107)$$

$$rate_ext : \text{ref. [2]}, \quad (108)$$

which agree with each other in general. The difference and the average of them are as follows respectively:

$$rate_{o-e} = (rate_ori - rate_ext)/2, \quad (109)$$

$$rate_{o+e} = (rate_ori + rate_ext)/2, \quad (110)$$

where $rate_{o-e}$ should agree with d_BD according to their definitions, and $rate_{o+e}$ represents the variation of biodiversity in the Phanerozoic eon. The outline of $rate_{o+e}$ indicates the declining Phanerozoic background extinction rates [34] [35] [36] [37] [38].

We define an essential biodiversity background variation rate by:

$$rate_essential = [amp(1) \cdot rate_{o+e}(1), amp(2) \cdot rate_{o+e}(2), ..., amp(5421) \cdot rate_{o+e}(5421)], \quad (111)$$

where

$$amp = \exp(k_{GS} \cdot (-t + 542.0)). \quad (112)$$

The outline of $rate_essential$ is generally horizontal (NOT declining). Especially, the peaks of the curve $rate_essential$ at P-Tr boundary and at K-Pg boundary are very high, which naturally divide the Phanerozoic eon into three climate phases (Fig 2c).

In the split scenario of biodiversification, we can explain the “declining” background extinction rates in the Phanerozoic eon. Firstly, there does not exist a tendency in the essential biodiversity background rate curve $rate_essential$. This essential rate was caused by the random tectonic contribution (no tendency) to the biodiversity evolution:

$$rate_essential = \frac{\text{variation of biodiversity}}{\text{tectonic contribution to biodiversity}}. \quad (113)$$

Then, the declining tendency in the observed background extinction or origination rates was caused by the genomic contribution to the biodiversity evolution:

$$rate_{o+e} = \frac{\text{variation of biodiversity}}{\text{tectonic contribution} + \text{genomic contribution to biodiversity}}. \quad (114)$$

It follows that (Fig 2c):

$$rate_{o+e} = \exp(-k_{GS} \cdot (-t + 542.0)) \cdot rate_{essential}, \quad (115)$$

where $rate_{o+e}$ is declining due to the factor $\exp(-k_{GS} \cdot (-t + 542.0))$.

The genomic contribution to the biodiversity plays a significant role in the robustness of biodiversity evolution: the random tectonic contribution can hardly wipe out all the life on the earth thanks for the exponential growth genomic contribution to the biodiversity evolution.

5.5 Calculating the origin time of taxa based on the overall trend of genome size evolution

5.5.1 The three-stage pattern in Metazoan origination

We can calculate the origin time of animal taxa according to the linear relationship between the origin time and the specific genome size. We obtained the specific genome sizes of the 19 taxa in the Animal Genome Size Database (Nematodes, Chordates, Sponges, Ctenophores, Tardigrades, Miscellaneous Inverts, Arthropod, Annelid, Myriapods, Flatworms, Rotifers, Cnidarians, Fish, Echinoderm, Molluscs, Bird, Reptile, Amphibian, Mammal):

$$G_{sp}^{animal}(\lambda^{animal}) = G_{mean_log}^{animal}(\lambda^{animal}) - \chi \cdot G_{sd_log}^{animal}(\lambda^{animal}), \quad (116)$$

where $\lambda^{animal} = 1, 2, \dots, 19$. We can obtain the origin order of these 19 taxa by comparing their specific genome sizes. Hence, we can classify these 19 taxa into Basal metazoa, Protostomia and Deuterostomia according to cluster analysis of their specific genome sizes (Data_3). Our result supports the three-stage pattern in Metazoan origination based on fossil records [39] [40] [41] [42] [43] [44] [45].

5.5.2 On angiosperm origination

Similarly, we can calculate the origin time of angiosperm taxa according to the linear relationship between the origin time and the specific genome size. We obtained the specific genome sizes of the 53 taxa of angiosperms in the Plant DNA C-value Database (we chose the taxa whose number of species is greater than 20 in the calculations):

$$G_{sp}^{angiosperm}(\lambda^{angiosperm}) = G_{mean_log}^{angiosperm}(\lambda^{angiosperm}) - \chi \cdot G_{sd_log}^{angiosperm}(\lambda^{angiosperm}), \quad (117)$$

where $\lambda^{angiosperm} = 1, 2, \dots, 53$. We can obtain the origin order of these 53 taxa by comparing their specific genome sizes. Hence, we can classify these 53 taxa into Dicotyledoneae and Monocotyledoneae (Data_3).

Note: The validity of our theory on genome size evolution is supported by its reasonable explanation of metazoan origination and angiosperm origination.

Notation: We denote the mean logarithm genome size, the standard deviation genome size and the specific genome sizes by concatenations for all the 19 animal taxa and the 53 plant taxa:

$$G_{mean_log} = [G_{mean_log}^{animal}, G_{mean_log}^{angiosperm}] \quad (118)$$

$$G_{sd_log} = [G_{sd_log}^{animal}, G_{sd_log}^{angiosperm}] \quad (119)$$

$$G_{sp} = [G_{sp}^{animal}, G_{sp}^{angiosperm}]. \quad (120)$$

5.6 The phylogenetic tree based on the correlation among genome size distributions

We found that the phylogenetic tree for taxa can be easily obtained based on the correlation coefficients among their genome size distributions. We denote the genome size distribution for a taxon λ by:

$$D_{gs}(\lambda, :) = [D_{gs}(\lambda, 1), D_{gs}(\lambda, 2), \dots, D_{gs}(\lambda, k), \dots, D_{gs}(\lambda, cutoff_{gs})], \quad (121)$$

where there are $D_{gs}(\lambda, k)$ species in taxon λ whose genome size is between $(k - 1) \cdot step_{gs}$ and $k \cdot step_{gs}$, the genome size step $step_{gs} = 0.01$ picogram (pg) and the genome size cutoff is $cutoff_{gs} =$

2000. Hence, we define the genome size distribution distance matrix $M_{gs}(\lambda_1, \lambda_2)$ among taxa by:

$$M_{gs}(\lambda_1, \lambda_2) = 1 - \text{corrcoef}(D_{gs}(\lambda_1, :), D_{gs}(\lambda_2, :)), \quad (122)$$

by which, we can draw the phylogenetic tree of the taxa.

We can obtain the genome size distributions $D_{gs}^P(\lambda, :)$ and consequently obtain the genome size distribution distance matrix $M_{gs}^P(\lambda_1, \lambda_2)$ among the above 7 taxa as follows:

$$M_{gs}^P(\lambda_1, \lambda_2) = 1 - \text{corrcoef}(D_{gs}^P(\lambda_1, :), D_{gs}^P(\lambda_2, :)), \quad (123)$$

where $\lambda_1, \lambda_2 = 1, 2, \dots, 7$. Hence, we can draw the phylogenetic tree of the 7 taxa based on M_{gs}^P (Fig S2c).

We can obtain the genome size distributions $D_{gs}^{animal}(\lambda, :)$ and consequently obtain the genome size distribution distance matrix $M_{gs}^{animal}(\lambda_1, \lambda_2)$ among the above 19 animal taxa as follows:

$$M_{gs}^{animal}(\lambda_1^{animal}, \lambda_2^{animal}) = 1 - \text{corrcoef}(D_{gs}^{animal}(\lambda_1^{animal}, :), D_{gs}^{animal}(\lambda_2^{animal}, :)), \quad (124)$$

where $\lambda_1^{animal}, \lambda_2^{animal} = 1, 2, \dots, 19$. Hence, we can draw the phylogenetic tree of the 19 taxa based on M_{gs}^{animal} (Fig 3c).

We can obtain the genome size distributions $D_{gs}^{angiosperm}(\lambda, :)$ and consequently obtain the genome size distribution distance matrix $M_{gs}^{angiosperm}(\lambda_1, \lambda_2)$ among the 25 angiosperm taxa (we chose 25 angiosperm taxa whose number of species is greater than 50 in the Plant DNA C-value database in order to obtain nontrivial distributions) as follows:

$$M_{gs}^{angiosperm}(\lambda_1^{angiosperm}, \lambda_2^{angiosperm}) = 1 - \text{corrcoef}(D_{gs}^{angiosperm}(\lambda_1^{angiosperm}, :), D_{gs}^{angiosperm}(\lambda_2^{angiosperm}, :)), \quad (125)$$

where $\lambda_1^{angiosperm}, \lambda_2^{angiosperm} = 1, 2, \dots, 25$. Hence, we can draw the phylogenetic tree of the 25 taxa based on $M_{gs}^{angiosperm}$ (Fig S2d).

These phylogenetic trees based on genome size distribution distance matrices generally agree with the traditional phylogenetic trees respectively, which is an evidence to show the close relationship between the genome evolution and the biodiversity evolution.

Software: PHYLIP to draw the phylogenetic trees (Neighbor-Joining) in this paper [46].

5.7 The varying velocity of molecular clock among taxa

The growth rates $k_{GS}(\lambda)$ of overall genome size evolution $OT_{taxa}(\lambda)$ for taxa λ are not constant, though we have an average growth rate k_{GS} for $OT-GS$. We have an approximate relationship that the earlier the origin time $T_{ori}(\lambda)$ is, the slower the growth rate $k_{GS}(\lambda)$ is:

$$(k_{GS}(\lambda) - k_{GS}) \cdot T_{ori}(\lambda) \doteq \hat{G}, \quad (126)$$

where the constant \hat{G} is the difference between the intercept of the overall trend of mean logarithm genome size OT_{mean_log} and the intercept of $OT-GS$.

5.8 The genomic curve and the genomic contribution to the biodiversity evolution

We define the genomic curve by a straight line with slope k_{GS} and the undetermined intercept b_{today} :

$$Curve_Genomic = k_{GS} \cdot (-t) + b_{today}, \quad (127)$$

which represents the exponential contribution to the biodiversity evolution.

6 Construction of the tectono-genomic curve

6.1 The synthesis scheme for the tectono-genomic curve

The above undetermined intercept of the genomic curve can be defined as:

$$b_{today} = Curve_Sepkoski(today) - Curve_Tectonic(today) \quad (128)$$

such that $Curve_TectonoGenomic(5421) = Curve_Sepkoski(5421)$.

We define the tectono-genomic curve by synthesizing the tectonic curve $Curve_Tectonic$ and the genomic curve $Curve_Genomic$ (Fig 1):

$$Curve_TectonoGenomic = \exp(Curve_Tectonic + Curve_Genomic), \quad (129)$$

which agrees very well with the Phanerozoic biodiversity curve *Curve_Sepkoski*:

$$Curve_TectonoGenomic \approx Curve_Sepkoski. \quad (130)$$

Thus, the Sepkoski curve based on fossil records can be explained by the tectono-genomic curve based on climatic, eustatic and genomic data.

6.2 The driving forces of biodiversity evolution at the molecular level and at the species level

Thus, we have explained the Sepkoski curve in the split scenario. The exponential growth part in the Phanerozoic biodiversity evolution was driven by the genome size evolution on one hand, and the variation of the the Phanerozoic biodiversity evolution was caused by the Phanerozoic sea level fluctuation and climate change on the other hand.

The successful explanation of the Phanerozoic biodiversity curve *Curve_Sepkoski* shows that the driving force of the biodiversity evolution is the tectono-genomic driving force. There are two independent tectonic and genomic driving forces in the biodiversity evolution. The first driving force originated from the plate tectonics movement at the species level; while the second driving force originated from the genome evolution at the molecular level.

7 The error analysis and reasonability analysis

7.1 The agreement between the Sepkoski curve and the tectono-genomic curve

7.1.1 The error analysis of the consensus climate curve

We obtain the first weighted average climate curve C_{w1} by choosing the corresponding $\Delta R(n)$, $n = 2, 3, 4$ as the weights $w1$ for C^1 , C^2 and C^3 as follows:

$$\begin{aligned} w1 &= [\Delta R(2), \Delta R(3), \Delta R(4)] / (\Delta R(2) + \Delta R(3) + \Delta R(4)) \\ &= [0.3454, 0.1611, 0.4935], \end{aligned} \quad (131)$$

hence,

$$C_{w1} = nondim(w1(1) \cdot C^1 + w1(2) \cdot C^2 + w1(3) \cdot C^3). \quad (132)$$

We obtain the second weighted average climate curve C_{w2} by choosing the corresponding correlation coefficients as the weights $w2$ for C^1 , C^2 and C^3 as follows:

$$\begin{aligned} w2 &= [corrcoef(Curve_CC, C^1), corrcoef(Curve_CC, C^2), \\ &\quad corrcoef(Curve_CC, C^3)] / \\ &\quad (corrcoef(Curve_CC, C^1) + corrcoef(Curve_CC, C^2) + \\ &\quad + corrcoef(Curve_CC, C^3)) \\ &= [0.4865, 0.2796, 0.2339], \end{aligned} \quad (133)$$

hence,

$$C_{w2} = nondim(w2(1) \cdot C^1 + w2(2) \cdot C^2 + w2(3) \cdot C^3). \quad (134)$$

We can obtain a weighted average climate curve C_w by choosing the average of $w1$ and $w2$ as the weights w for C^1 , C^2 and C^3 as follows:

$$\begin{aligned} w &= (w1 + w2) / 2 \\ &= [0.4159, 0.2204, 0.3637], \end{aligned} \quad (135)$$

hence,

$$C_w = nondim(w(1) \cdot C^1 + w(2) \cdot C^2 + w(3) \cdot C^3), \quad (136)$$

which agrees with $Curve_CC$.

The weights $w1$ or $w2$ can be referred to as credibilities for the independent curves C^1 , C^2 and C^3 . Both of C_{w1} and C_{w2} are reasonable estimations of the Phanerozoic climate. So, we can consider the zone between C_{w1} and C_{w2} as the error range of $Curve_CC$, whose upper range C_{upper} and lower range C_{lower} are about as follows (Fig S1b):

$$C_{upper} = max(C_{w1}, C_{w2}), \quad (137)$$

$$C_{lower} = min(C_{w1}, C_{w2}). \quad (138)$$

7.1.2 The error analysis of the consensus sea level curve

We obtain the weighted average sea level curve S_w by choosing the corresponding $\Delta R(n)$, $n = 10, 11$ as the weights w' for S^1 and C^2 as follows:

$$\begin{aligned} w' &= [\Delta R(10), \Delta R(11)] / (\Delta R(10) + \Delta R(11)) \\ &= [0.4872, 0.5128], \end{aligned} \quad (139)$$

hence,

$$S_w = \text{nondim}(w'(1) \cdot S^1 + w'(2) \cdot S^2), \quad (140)$$

which agrees with *Curve_SL*.

We can consider the zone between S^1 and S^2 as the error range of *Curve_SL*, whose upper range S_{upper} and lower range S_{lower} are about as follows (Fig S1c):

$$S_{upper} = \max(S^1, S^2), \quad (141)$$

$$S_{lower} = \min(S^1, S^2). \quad (142)$$

7.1.3 The error analysis of the Sepkoski curve

We can consider the zone between *Curve_S_AllGenera* and *Curve_S_WellResolvedGenera* as the error range of *Curve_Sepkoski* (Fig 1):

$$\textit{Curve_S_AllGenera} : \text{ref. [3]}, \quad (143)$$

$$\textit{Curve_S_WellResolvedGenera} : \text{ref. [3]}, \quad (144)$$

where *Curve_S_AllGenera* is the Phanerozoic biodiversity curve based on all the genera in Sepkoski's data and *Curve_S_WellResolvedGenera* is the Phanerozoic biodiversity curve based on well resolved genera in Sepkoski's data.

7.1.4 The error analysis of the tectono-genomic curve

In consideration of the error ranges of *Curve_CC* and *Curve_SL* as well as their phase relationships, we define the associate upper tectono-genomic curve *Curve_TG_upper_0* and the

associate lower tectono-genomic curve $Curve_TG_lower_0$ as follow:

$$Curve_TG_upper_0 = [(S_{upper}([P]) + C_{upper}([P]))/2, (S_{upper}([MC]) - C_{lower}([MC]))/2], \quad (145)$$

$$Curve_TG_lower_0 = [(S_{lower}([P]) + C_{lower}([P]))/2, (S_{lower}([MC]) - C_{upper}([MC]))/2]. \quad (146)$$

Furthermore, in the similar process and with the same parameters in construction of the tectono-genomic curve, we can obtain the upper range and the lower range of the tectono-genomic curve as follows (Fig 1):

$$Curve_TG_upper = \exp(Curve_Genomic + a_{std} \cdot (Curve_TG_upper_0 - \text{mean}(Curve_TG_upper_0))), \quad (147)$$

$$Curve_TG_lower = \exp(Curve_Genomic + a_{std} \cdot (Curve_TG_lower_0 - \text{mean}(Curve_TG_lower_0))). \quad (148)$$

7.2 The reasonability of the principal conjectures

7.2.1 Reasonability of the climate phase reverse based on $r_{\mu\nu}^{\rho}(n)$

We can obtain the following 10 groups of curves to describe the Phanerozoic climate, sea level and biodiversity:

$$\begin{array}{lll} n = 1 & : & Curve_SL, Curve_BD, Curve_CC \\ n = 2 & : & Curve_SL, Curve_BD, C^1 \\ n = 3 & : & Curve_SL, Curve_BD, C^2 \\ n = 4 & : & Curve_SL, Curve_BD, C^3 \\ n = 5 & : & Curve_SL, Curve_BD, C_{w1} \\ n = 6 & : & Curve_SL, Curve_BD, C_{w2} \\ n = 7 & : & Curve_SL, Curve_BD, C_w \\ n = 8 & : & S^1, Curve_BD, Curve_CC \\ n = 9 & : & S^2, Curve_BD, Curve_CC \\ n = 10 & : & S_w, Curve_BD, Curve_CC \end{array} \quad (149)$$

And we can obtain the correlation coefficients $r_{\mu\nu}^{\rho}(n)$ among these groups of curves (Data_2), where

$$\mu, \nu = S, B, C, C^1, C^2, C^3, C_{w1}, C_{w2}, C_w, S^1, S^2, S_w \quad (150)$$

for the curves $Curve_SL$, $Curve_BD$, $Curve_CC$, C^1 , C^2 , C^3 , C_{w1} , C_{w2} , C_w , S^1 , S^2 and S_w respectively.

We can define the corresponding average correlation coefficients for all the 10 groups of curves ($n = 1, 2, \dots, 10$) as follows:

$$R^+(n), R^-(n), \Delta R(n), Q(n), Q'(n), \Delta Q(n). \quad (151)$$

The conclusions on the climate phases CP I, CP II and CP III based on the first group of curves ($n = 1$) still hold for the cases of the other groups of curves ($n = 2, 3, \dots, 10$). Namely, the following equations holds in general:

$$r_{SB}^P(n) > 0 \quad (152)$$

$$r_{BC}^P(n) > 0 \quad (153)$$

$$r_{CS}^P(n) > 0 \quad (154)$$

for CP I,

$$r_{SB}^M(n) > 0 \quad (155)$$

$$r_{BC}^M(n) < 0 \quad (156)$$

$$r_{CS}^M(n) < 0 \quad (157)$$

for CP II, and

$$r_{SB}^C(n) < 0 \quad (158)$$

$$r_{BC}^C(n) < 0 \quad (159)$$

$$r_{CS}^C(n) > 0 \quad (160)$$

for CP III.

Furthermore, we have

$$R^+(n) > 0 \text{ (tend to be equal to 1)} \quad (161)$$

$$R^-(n) < 0 \text{ (tend to be equal to } -1) \quad (162)$$

$$\Delta R(n) \gg 0 \quad (163)$$

$$Q(n) \sim 1 \text{ (tend to be equal to 1)} \quad (164)$$

$$Q'(n) \sim 0 \text{ (tend to be equal to 0)} \quad (165)$$

$$\Delta Q(n) > 0 \quad (166)$$

which shows that the division of three climate phases is an essential property in the evolution rather than just random phenomenon in math games.

The explanation of the P-Tr extinction based on the phase reverse at P-Tr boundary is therefore valid regardless the disagreement in the raw data of the Phanerozoic climate and sea level. Especially, $\Delta R(1)$ and $\Delta Q(1)$ are relatively the maximum among these 10 groups of curves, hence we chose the optimal first group of curves to describe the Phanerozoic climate, sea level and biodiversity throughout this paper.

The climate system was not stationary when coupling with the other earth's spheres around P-Tr boundary. We calculate the correlation coefficients $r_{\mu\nu}^\rho$, where $\rho = P \setminus L, L, L.M.Tr, M \setminus L.M.Tr$ in detail around P-Tr boundary. The curve *Curve_{CC}* varies instead in the opposite phase with *Curve_{SL}* and *Curve_{BD}* in Lopingian yet; and it varies instead in the same phase with *Curve_{SL}* and *Curve_{BD}* in Lower and Middle Triassic.

7.2.2 Reasonability of the split scenario

We summarize the reasons to propose the split scenario in observing the biodiversity evolution as follows.

(1) Evidences to support the close relationship between the genome evolution and the biodiversity evolution:

- Exponential growth in both the genome size evolution and the biodiversity evolution
- Agreement between genome size growth rate k_{GS} and biodiversity growth rate k_{BD} , namely $\tau_{GS} \approx \tau_{BD}$
- Favorable phylogenetic trees based on $M_{gs}^P, M_{gs}^{animal}, M_{gs}^{angiosperm}, M_{ci}^{all}, M_{ci}^{euk}$

- Verification of the three-stage pattern in Metazoan origination and the classification of dicotyledoneae and monocotyledoneae in angiosperm origination based on the overall trend in genome size evolution
- Reasonable extrapolation of the overall trend in genome size evolution obtained in Phanerozoic eon to the Precambrian period
- The relationship between phylogenetic trees of species by M_{ci} and the evolutionary tree of codons by M_{codon} based on the same matrix Δ .

(2) Successful applications of the split scenario:

- Explanation of the Sepkoski curve by the tectono-genomic curve in the split scenario
- Error analysis agreement between *Curve_Sepkoski* and *Curve_TectonoGenomic*
- Explanation of the declining Phanerozoic background extinction rates
- Explanation of the robustness of biosphere in the tremendously changing environment.

8 The genetic code evolution as the initial driving force in the biodiversity evolution

8.1 The evolutionary relationship between the tree of life and the tree of codon

8.1.1 The codon interval distribution D_{ci}

We can obtain both the phylogenetic tree of species and the evolutionary tree of 64 codons based on the codon interval distributions in the whole genomes. For a certain species α and a certain codon n_c ($n_c = 1, 2, \dots, 64$ for 64 codons), we define the “codon interval” $I(n_c, \alpha, p)$ as the distance between a pair (p) of neighboring codon n_c ’s in the whole genome sequence. We define the codon

interval distribution

$$D_{ci}(n_c, \alpha, :) = [D_{ci}(n_c, \alpha, 1), D_{ci}(n_c, \alpha, 2), \dots, D_{ci}(n_c, \alpha, cutoff_{ci})]. \quad (167)$$

as the distribution of all the codon intervals $I(n_c, \alpha, p)$ in the whole genome sequence (reading in only one direction), where there are $D_{ci}(i)$ pairs of codon n_c 's with the distance i (the cutoff of distance in the calculations is set as $cutoff_{ci} = 1000$ bases). For a group of N species, there are $64 \times N$ $cutoff_{ci}$ -dim vectors $D_{ci}(n_c, \alpha, :)$.

Example: The “GGC” codon interval distribution of the following “genome α_0 ” is $D_{ci}(\text{“GGC”}, \alpha_0, :) = [0, 0, 1, 3, 5, 1, 0, 0, 0, 0]$, where $cutoff_0 = 10$.

GGCAUGGCUUGGCAUCGGCAGGCAUGGCAGGCGGCAUGGCAGGCUUGGCAGCA

And the “GCA” codon interval distribution of the same “genome α_0 ” is $D_{ci}(\text{“GCA”}, \alpha_0, :) = [0, 0, 1, 1, 2, 1, 1, 0, 1, 1]$.

GGCAUGGCUUGGCAUCGGCAGGCAUGGCAGGCGGCAUGGCAGGCUUGGCAGCA

Hence, the correlation coefficient between $D_{ci}(\text{“GGC”}, \alpha_0, :)$ and $D_{ci}(\text{“GCA”}, \alpha_0, :)$ is

$$corrcoef(D_{ci}(\text{“GGC”}, \alpha_0, :), D_{ci}(\text{“GCA”}, \alpha_0, :)) = 0.7235.$$

8.1.2 The codon interval correlation matrix Δ

The codon interval correlation matrix $\Delta(n_c, \alpha, \beta)$ for a group of N species is defined as the $64 \times N \times N$ matrix of the correlation coefficients between pairs of vectors $D_{ci}(n_c, \alpha)$ and $D_{ci}(n_c, \beta)$:

$$\Delta(n_c, \alpha, \beta) = corrcoef(D_{ci}(n_c, \alpha, :), D_{ci}(n_c, \beta, :)). \quad (168)$$

8.1.3 Calculating the codon interval distance matrix of species M_{ci} according to Δ

We can obtain the $N \times N$ codon interval distance matrix $M_{ci}(\alpha, \beta)$ of the N species by averaging the $64 \times N \times N$ correlation coefficients with respect to the 64 codons:

$$M_{ci}(\alpha, \beta) = 1 - \frac{1}{64} \sum_{n_c=1}^{64} \Delta(n_c, \alpha, \beta). \quad (169)$$

Hence, we can draw the phylogenetic tree of N species based on M_{ci} .

The method to obtain phylogenetic trees of species based on the codon interval distance matrices is valid not only for eukarya but also for bacteria, archaea and virus. The phylogenetic trees of species based on the codon interval distance matrices generally agree with the traditional phylogenetic trees respectively, which is also an evidence to show the close relationship between the genome evolution and the biodiversity evolution.

8.1.4 Calculating the distance matrix of codons M_{codon} according to Δ

We can obtain the 64×64 distance matrix of codons M_{codon} by averaging the $64 \times N \times N$ correlation coefficients with respect to the N species:

$$M_{codon}(n_c, n'_c) = 1 - corrcoeff(\Delta(n_c, :, :), \Delta(n'_c, :, :)). \quad (170)$$

Hence, we can draw the evolutionary tree of 64 codons based on M_{codon} .

The evolutionary tree of codons based on M_{codon} agrees with the traditional understanding of the genetic code evolution. Thus, we can obtain both the phylogenetic tree of species and the evolutionary tree of 64 codons based on the same codon interval correlation matrix Δ . This is an evidence to show the close relationship between the genetic code evolution and the biodiversity evolution. The principal rules in the biodiversity evolution may concern the primordial molecular evolution.

8.2 The tree of life and the tree of codon (example 1)

Based on the genomes of 748 bacteria, 55 archaea, 16 eukaryotes and 133 viruses (GeneBank, up to 2009), we can obtain the codon interval correlation matrices Δ^{all} . For the eukaryotes with several chromosomes, the codon interval distributions are obtained by averaging the codon interval distributions with respect to the chromosomes of the certain species. Consequently, we can obtain the reasonable phylogenetic tree of these species (Fig S3a) and the reasonable tree of 64 codons

(Fig 4a) by calculating $M_{ci}^{all}(\alpha, \beta)$ and $M_{codon}^{all}(n_c, n'_c)$ from Δ^{all} :

$$M_{ci}^{all}(\alpha, \beta) = 1 - \frac{1}{64} \sum_{n_c=1}^{64} \Delta^{all}(n_c, \alpha, \beta), \quad (171)$$

and

$$M_{codon}^{all}(n_c, n'_c) = 1 - corrcoeff(\Delta^{all}(n_c, :, :), \Delta^{all}(n'_c, :, :)). \quad (172)$$

8.3 The tree of life and the tree of codon (example 2)

Based on the genomes of 16 eukaryotes, we can obtain the codon interval correlation matrices Δ^{euk} . Consequently, we can obtain the reasonable phylogenetic tree of these 16 eukaryotes (Fig 4c) and the reasonable tree of 64 codons (Fig S3b) by calculating $M_{ci}^{euk}(\alpha, \beta)$ and $M_{codon}^{euk}(n_c, n'_c)$ from Δ^{euk} . If there are several chromosomes ($chr(\alpha) = 1, 2, \dots, c_m(\alpha)$) in the genome of eukaryote α , the codon interval distributions of the chromosomes of species α are $D_{ci}^{euk}(n_c, \alpha, chr(\alpha), :)$. The codon interval correlation matrix is:

$$\Delta^{euk}(n_c, \alpha, chr(\alpha), \beta, chr(\beta)) = corrcoeff(D_{ci}^{euk}(n_c, \alpha, chr(\alpha), :), D_{ci}^{euk}(n_c, \beta, chr(\beta), :)). \quad (173)$$

Consequently, we can calculating the codon interval distance matrix of species:

$$M_{ci}^{euk}(\alpha, \beta) = 1 - \frac{1}{64} \sum_{n_c=1}^{64} \left(\frac{1}{c_m(\alpha)} \frac{1}{c_m(\beta)} \sum_{chr(\alpha)=1}^{c_m(\alpha)} \sum_{chr(\beta)=1}^{c_m(\beta)} \Delta^{euk}(n_c, \alpha, chr(\alpha), \beta, chr(\beta)) \right) \quad (174)$$

and the distance matrix of codons:

$$M_{codon}^{euk}(n_c, n'_c) = 1 - corrcoeff(\Delta^{euk}(n_c, :, :, :), \Delta^{euk}(n'_c, :, :, :)) \quad (175)$$

The phylogenetic tree of eukaryotes by this chromosome average method (for M_{ci}^{euk}) generally agrees with the tree by the chromosome average method (for M_{ci}^{all}).

8.4 Three periods in genetic code evolution

We arrange the 64 codons in the “codon_aa” order by considering the codon chronology order firstly and considering the amino acid chronology order secondly according to the results in [27]:

codon chronology:

$$\begin{aligned}
 & (1)GGC, GCC, \quad (2)GUC, GAC, \quad (3)GGG, CCC, \quad (4)GGA, UCC, \\
 & (5)GAG, CUC, \quad (6)GGU, ACC, \quad (7)GCG, CGC, \quad (8)GCU, AGC, \\
 & (9)GCA, UGC, \quad (10)CCG, CGG, \quad (11)CCU, AGG, \quad (12)CCA, UGG, \\
 & (13)UCG, CGA, \quad (14)UCU, AGA, \quad (15)UCA, UGA, \quad (16)ACG, CGU, \\
 & (17)ACU, AGU, \quad (18)ACA, UGU, \quad (19)GAU, AUC, \quad (20)GUG, CAC, \\
 & (21)CUG, CAG, \quad (22)AUG, CAU, \quad (23)GAA, UUC, \quad (24)GUA, UAC, \\
 & (25)CUA, UAG, \quad (26)GUU, AAC, \quad (27)CUU, AAG, \quad (28)CAA, UUG, \\
 & (29)AUA, UAU, \quad (30)AUU, AAU, \quad (31)UUA, UAA, \quad (32)UUU, AAA,
 \end{aligned} \tag{176}$$

amino acid chronology:

$$\begin{aligned}
 & (1) G, (2) A, (3) V, (4) D, (5) P, (6) S, (7) E, (8) L, (9) T, (10) R, \\
 & (11) I, (12) Q, (13) N, (14) K, (15) H, (16) F, (17) C, (18) M, (19) Y, (20) W.
 \end{aligned} \tag{177}$$

We define the average correlation curves Hurdle curve and Barrier curve as follows:

$$Hurdle(\alpha) = \text{mean}(M_{\text{codon}}(\alpha, :)), \tag{178}$$

$$Barrier(\alpha) = \text{mean}(\{M_{\text{codon}}(\beta, \beta') : |\beta - \alpha| \leq n_{\text{barr}} \text{ and } |\beta' - \alpha| \leq n_{\text{barr}}\}), \tag{179}$$

where $n_{\text{barr}} = 8$.

According to the observations of the certain positions of the three terminal codons in the evolutionary tree of codons (Fig 4a, S3b) and the certain shapes of the Hurdle curve and the Barrier curve (Fig 4b, S3c), we propose three periods in the genetic code evolution:

$$(1) \text{ initial period, } (2) \text{ transition period, and } (3) \text{ fulfillment period,} \tag{180}$$

which are separated by the three terminal codons and correspond to the origination of three terminal codons respectively. We observe that the curve *Barrier* begins at a level of *Barrier* ~ 0.4 , then overcome a “barrier” of level *Barrier* ~ 0.5 , and at last reach a low place of level *Barrier* ~ 0.3 (Fig 4b). Between the initial period and the fulfillment period, we can observe some considerably higher values in the curves *Barrier* and *Hurdle*, which indicates a “barrier” in the middle period

of the genetic code evolution. The overall trend of the curve *barrier* is declining. This “barrier” in the curve *Barrier* corresponds to the narrow palace in the middle of the tree of 64 codons based on M_{codon} .

9 A heuristic model on the coupled earth spheres

9.1 The strategy of biodiversification

The robustness of biodiversification was ensured by the genomic contributions, without which the biodiversity on the earth can hardly survive the tremendous environmental changes. The mechanism of genome evolution is independent from the rapid environmental change during mass extinctions, which ensures the continuity of the evolution of life: all the phyla survived from the Five Big mass extinctions; more families (in ratio) survived from the mass extinctions than genera. The mass extinctions had only influenced some non-fatal aspects of the living system (e.g. wipeout of some genera or families), whose influence for the vital or more essential aspects of living system (e.g. the advancement aspect) was limited. The living system seems to be able to respond freely to any possible environmental changes on the earth. The sustainable development of the living system in the high risk earth environment was ensured at the molecular level rather than at the species level.

9.2 The tectonic timescale coupling of earth’s spheres

The three patterns CP I, CP II and CP III in the Phanerozoic eon indicate the tectonic timescale coupling of earth’s spheres. The driving force in the biodiversity evolution should be explained in a tectonic timescale dynamical mechanism. Although the P-Tr mass extinction happened rapidly within several 10^4 years, its cause should be explained in a broader context at the tectonic timescale. Overemphasis of the impacts of occasional events did not quite touch the core of the biodiversity evolution.

9.3 A triple pendulum model to explain the climate phase reverse event

The phase relationship among *Curve_{BD}*, *Curve_{SL}* and *Curve_{CC}* can be simulated by a triple pendulum model (Fig S1d) with the coupling constants k_1 , k_2 and a varying coupling $k_3(t) = (1 - \epsilon \arctan(t/t_0)/(\pi/2)) \cdot k_3$:

$$\begin{cases} \frac{d^2}{dt^2}\xi = -\xi - k_1(\xi - \eta) - k_3(t)(\xi - \zeta) \\ \frac{d^2}{dt^2}\eta = -\eta - k_2(\eta - \zeta) - k_1(\eta - \xi) \\ \frac{d^2}{dt^2}\zeta = -\zeta - k_3(t)(\zeta - \xi) - k_2(\zeta - \eta). \end{cases} \quad (181)$$

This model shows that the climate phase reverse can achieve by just varying the coupling $k_3(t)$ from $k_3(1 + \epsilon)$ to $k_3(1 - \epsilon)$, $\epsilon \ll 1$.

References

- [1] Sepkoski, J. J., Jr. A compendium of fossil marine animal genera. *Bulletins of American Paleontology* No. 363 (2002).
- [2] Bambach, R. K. et al. Origination, extinction, and mass depletions of marine diversity. *Paleobiology* 30, 522-542 (2004).
- [3] Rohde, R. A., Muller, R. A. Cycles in fossil diversity. *Nature* 434, 208-210 (2005).
- [4] Berner, R. A. The carbon cycle and CO_2 over Phanerozoic time: the role of land plants. *Phil. Trans. R. Soc. Lond. B.* 353, 75-82 (1998).
- [5] Boucot, A. J., Gray, J. A critique of Phanerozoic climatic models involving changes in the CO_2 content of the atmosphere. *Earth-Science Reviews* 56, 1-159 (2001).
- [6] Boucot, A. J. et al. *Reconstruction of the Phanerozoic Global Paleoclimate* (Science Press, Beijing, 2009).
- [7] Raymo, M. E. Geochemical evidence supporting T. C. Chamberlin's theory of glaciation. *Geology* 19, 344-347 (1991).
- [8] Hallam, A. *Phanerozoic Sea Level Changes* (Columbia Univ. Press, New York, 1992).
- [9] Haq, B. U. et al. Chronology of fluctuating sea levels since the triassic. *Science* 235, 1156-1167 (1987).
- [10] Haq, B. U., Schutter, S. R. A Chronology of Paleozoic Sea-Level Changes. *Science* 322, 64-68 (2008).
- [11] Hewzulla, D. et al. Evolutionary patterns from mass originations and mass extinctions. *Phil. Trans. R. Soc. Lond. B* 354, 463-469 (1999).

- [12] Sharov, A. A. Genome increases as a clock for the origin and evolution of life. *Biology Direct* 1, 17 (2007).
- [13] Li, D. J., Zhang, S. The Cambrian explosion triggered by critical turning point in genome size evolution. *Biochemical and Biophysical Research Communications* 392, 240-245 (2010).
- [14] Raup, D. M., Sepkoski, J. J., Jr. Mass extinctions in the marine fossil record. *Science* 215, 1501-1503 (1982).
- [15] Newman, M. E. J., Eble, G. J. Decline in extinction rates and scale invariance in the fossil record. *Paleobiology* 25, 434-439 (1999).
- [16] Berner, R. A., Kothavala, Z. GEOCARB III: a revised model of atmospheric CO_2 over phanerozoic time. *American Journal of Science* 301, 182-204 (2001).
- [17] Berner, R. A. et al. Phanerozoic atmospheric oxygen. *Annu. Rev. Earth Planet Sci.* 31, 105-134 (2003).
- [18] Jin, Y. G. Two phases of the end-Permian extinction. *Palaeoworld* 1, 39 (1991)
- [19] Jin, Y. G. The pre-Lopingian benthose crisis. *Compte Rendu, the 12th ICC-P* 2, 269-278 (1993).
- [20] Stanley, S. M., Yang, X. A double mass extinction at the end of the Paleozoic era. *Science* 266, 1340-1344 (1994).
- [21] Shen, S. et al. Calibrating the End-Permian Mass Extinction. *Science* 334, 1367-1372 (2011).
- [22] Jin, Y. G. et al. Pattern of Marine Mass Extinction Near the Permian-Triassic Boundary in South China. *Science* 289, 432-436 (2000).
- [23] Xie, S. et al. Two episodes of microbial change coupled with Permo/Triassic faunal mass extinction. *Nature* 434, 494-497 (2005).
- [24] Chen, Z., Benton, M. J. The timing and pattern of biotic recovery following the end-Permian mass extinction. *Nature Geoscience* 5, 375-383 (2012).
- [25] Renne, P. R., Basu, A. R. Rapid eruption of the Siberia Traps flood basalts at the Permo-Triassic boundary. *Science* 253, 176-179 (1991).
- [26] Campbell, I. H. et al. Synchronism of the Siberia Traps and the Permian-Triassic boundary. *Science* 258, 1760-1763 (1992).
- [27] Trifonov, E. N. et al. Primordia vita. deconvolution from modern sequences. *Orig. Life Evol. Biosph* 36, 559-565 (2006).
- [28] Trifonov, E. N. et al. Distinc stage of protein evolution as suggested by protein sequence analysis. *J. Mol Evol* 53, 394-401 (2001).
- [29] Wong, J. T.-F., Lazcano, A. *Prebiotic Evolution and Astrobiology* (Landes Bioscience, Austin Texas, 2009).
- [30] Shu, D. Cambrian explosion: Birth of tree of animals. *Gondwana Research* 14, 219-240 (2008).

- [31] Gregory, T.R. Animal Genome Size Database. <http://www.genomesize.com> (2012).
- [32] Bennett, M.D., Leitch, I.J. Plant DNA C-values database (release 5.0, Dec. 2010) <http://www.kew.org/cvalues/> (2010).
- [33] Veizer, J. et al. $^{87}\text{Sr}/^{86}\text{Sr}$, $\delta^{13}\text{C}$ and $\delta^{18}\text{O}$ evolution of Phanerozoic seawater. *Chemical Geology* 161, 59-88 (1999).
- [34] Flessa, K. W., Jablonski, D. Declining Phanerozoic background extinction rates: effect of taxonomic structure. *Nature* 313, 216-218 (1985).
- [35] Van Valen, L. How constant is extinction? *Evol. Theory* 7, 93-106 (1985).
- [36] Sepkoski, J. J. Jr. A model of onshore-offshore change in faunal diversity. *Paleobiology* 17, 58-77 (1991).
- [37] Gilinsky, N. L. Volatility and the Phanerozoic decline of background extinction intensity. *Paleobiology* 20, 445-458 (1994).
- [38] Alroy, J. Equilibrial diversity dynamics in north American mammals, in McKinney, M. L., Drake, J. A. ed. *Biodiversity Dynamics: Turnover of Populations, Taxa, and Communities* (Columbia Univ. Press, New York, 1998).
- [39] Conway-Morris, S. The fossil record and the early evolution of the metazoa. *Nature* 361, 219-225 (1993).
- [40] Conway-Morris, S. The Burgess shale fauna and the Cambrian explosion. *Science*, 339-346 (1989).
- [41] Budd, G., Jensen, S. A critical reappraisal of the fossil record of the bilaterian phyla. *Biological Review* 75, 253-295 (2000).
- [42] Shu, D. On the phylum vetulicolia. *Chinese Science Bulletin* 50, 2342-2354 (2005).
- [43] Shu, D. et al. Ancestral echinoderms from the Chengjiang deposits of China. *Nature* 430, 422-428 (2004).
- [44] Valentine, J. W. How were vendobiont bodies patterned? *Palaeobiology* 27, 425-428 (2001).
- [45] Shu, D. et al. Restudy of cambrian explosion and formation of animal tree. *ACTA Palaeontologica Sinica* 48, 414-427 (2009).
- [46] Felsenstein J. Evolutionary trees from DNA sequences: a maximum likelihood approach. *J Mol Evol* 17, 368-76 (1981).

*E-mail: dirson@mail.xjtu.edu.cn

Acknowledgements My warm thanks to Jinyi Li for valuable discussions. Supported by the Fundamental Research Funds for the Central Universities.

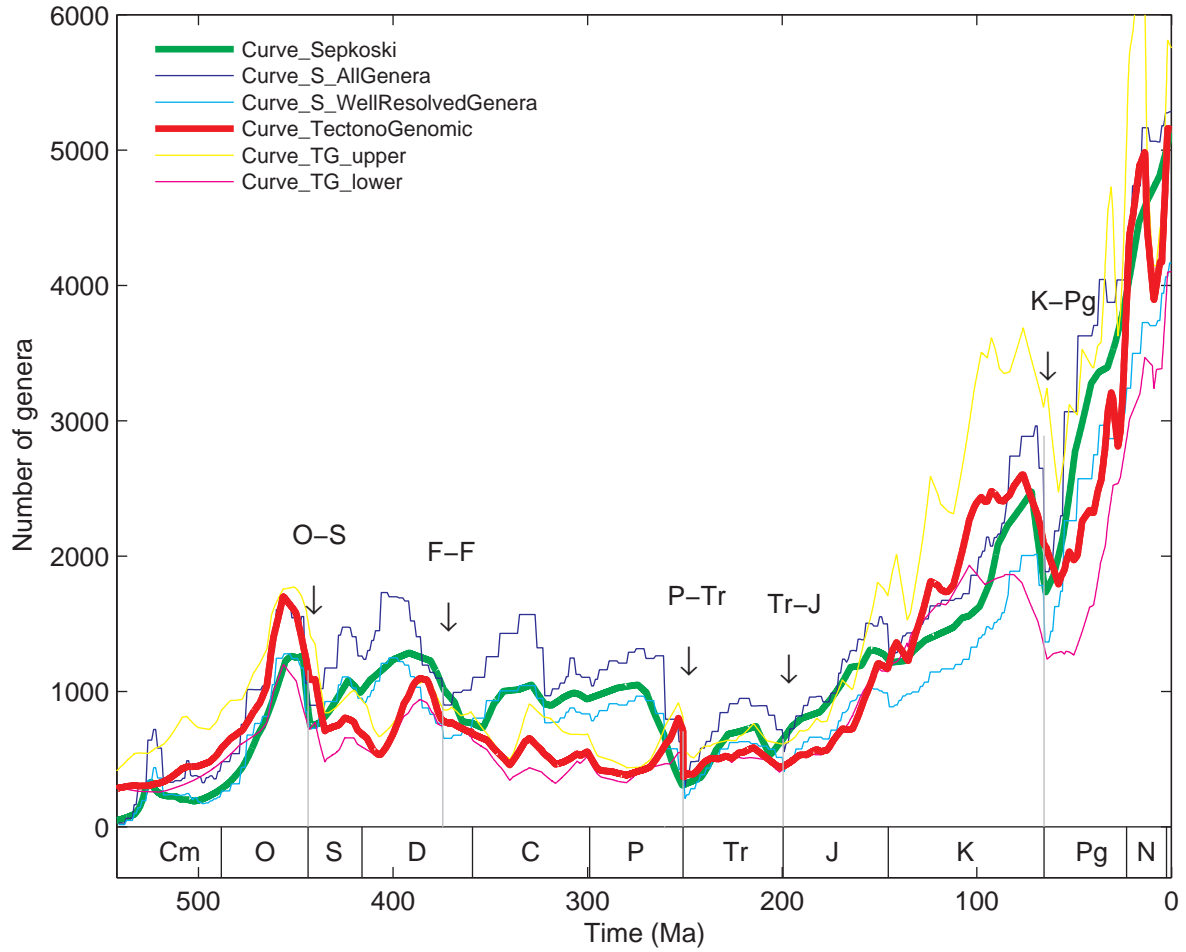


Figure 1: **Explanation of the Sepkoski curve by a tectono-genomic curve.** *Curve_TectonoGenomic* generally agrees with *Curve_Sepkoski* not only in overall trends but also in detailed fluctuations (including some very detailed fluctuation agreement with *Curve_S_AllGenera*). The error range of the Sepkoski curve is about between *Curve_S_AllGenera* and *Curve_S_WellResolvedGenera*. The error range of the tectono-genomic curve is about between *Curve_TG_upper* and *Curve_TG_lower*.

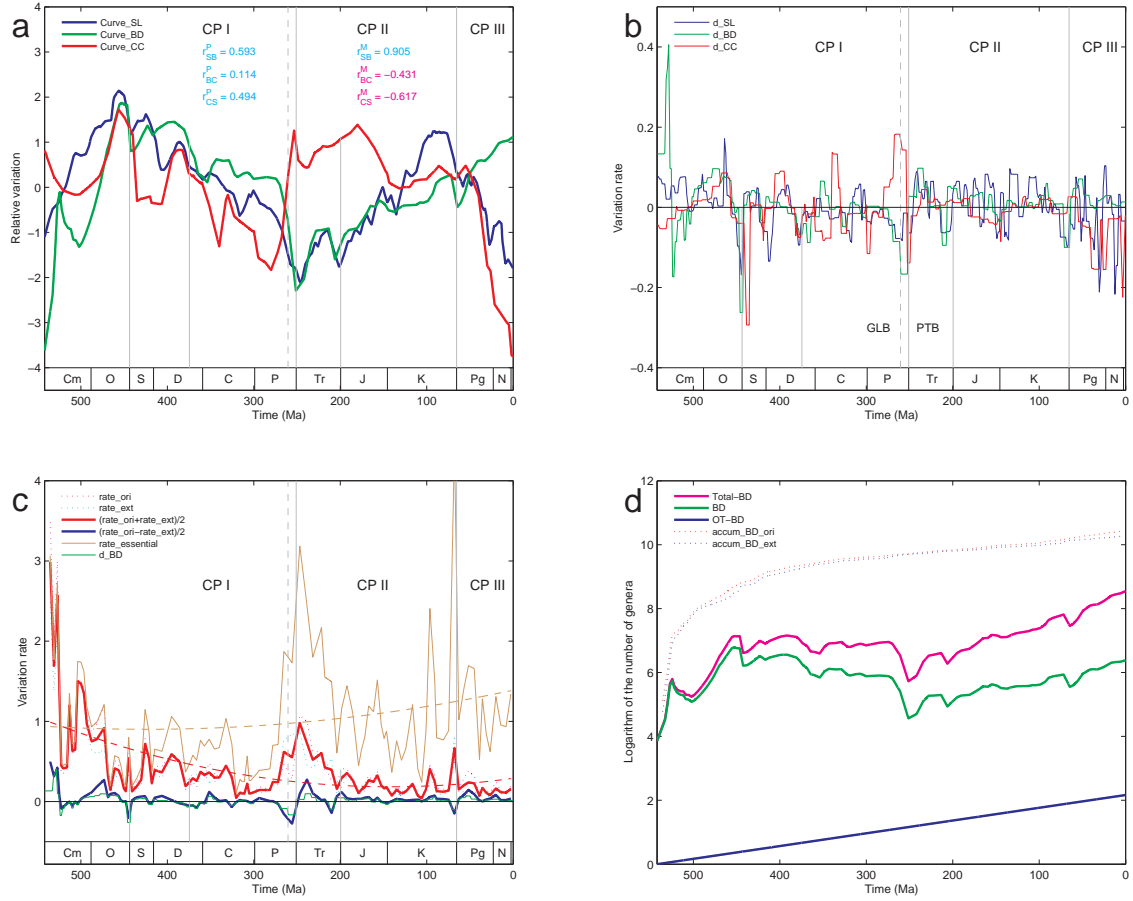


Figure 2: The tectonic contribution to the fluctuations in the biodiversity evolution. **a** The consensus climate curve, the consensus sea level curve and the biodiversification curve. There are three climate phases CP I, II, III naturally corresponds to Paleozoic, Mesozoic and Cenozoic respectively. *Curve_{BD}* generally agrees with *Curve_{SL}*. *Curve_{BD}* only agrees with *Curve_{CC}* in the Paleozoic era, but varies oppositely with *Curve_{CC}* in the Mesozoic and Cenozoic eras in general. **b** Climate, sea level and biodiversification variation rate curves. We can observe a sharp upward peak at GLB and a sharp downward peak at PTB on the curve *d_{CC}*. **c** Explanation of the declining Phanerozoic background extinction rates. The overall trend of the essential biodiversity background variation rate *rate_{essential}* is about horizontal, while the overall trend of the origination and extinction rate curves *rate_{ori}*, *rate_{ext}* and their average decline due to the increasing genomic contribution. **d** The total biodiversity curve *Total-BD* is equal to its net variation *BD* plus its overall trend *OT-BD*. Also, the overall trends of accumulation origination and extinction biodiversity curves are exponential.

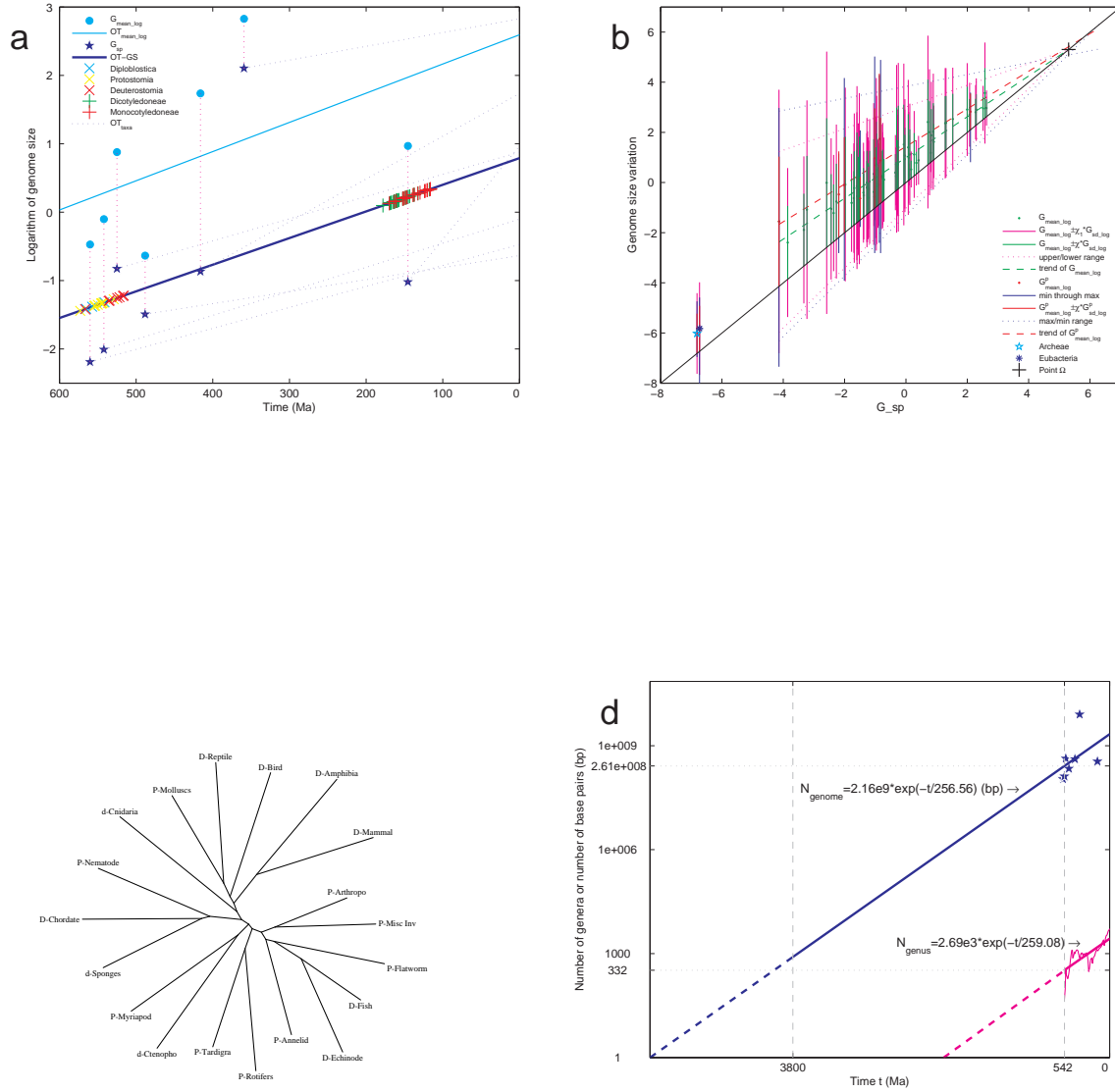


Figure 3: The genomic contribution to the overall trend of the biodiversity evolution. **a** The overall trend in the genome size evolution and its applications: (i) Prediction of origin time of taxa in Diploblostica, Protostomia and Deuterostomia indicates three-stage pattern in the metazoan origination; (ii) Prediction of origin time of angiosperm taxa differ between Dicotyledoneae and Monocotyledoneae. **b** Proof of the log-normal distribution of genome size in taxa by the common intersection point Ω . **c** The phylogenetic tree of animal taxa obtained by M_{gs}^P . **d** Agreement between the “e-folding” time τ_{BD} in biodiversity evolution and the “e-folding” time τ_{GS} in genome size evolution. Also, reasonable extrapolation of the overall trend of the genome size evolution obtained in the Phanerozoic eon to the Precambrian periods.

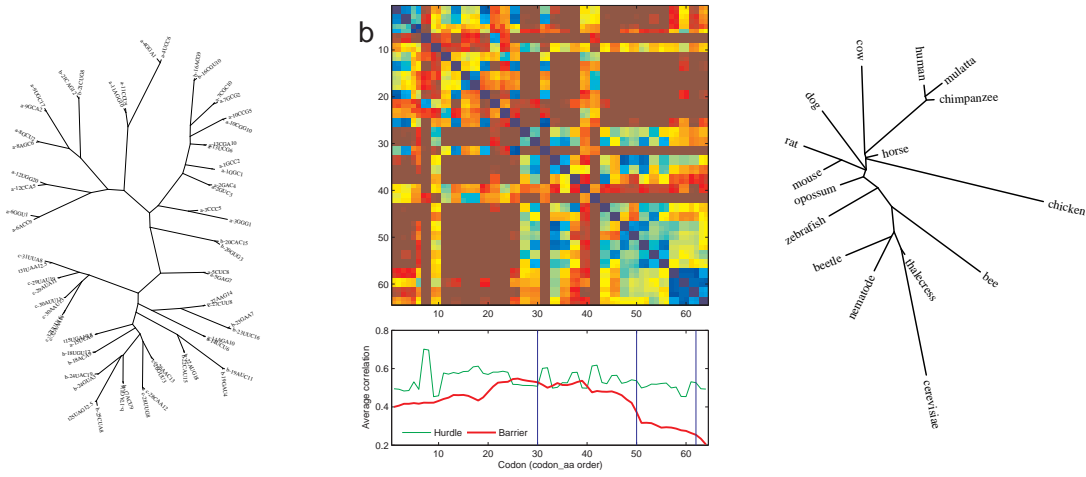


Figure 4: **Relationship between the molecular evolution and the biodiversity evolution.** **a** The evolutionary tree of codons obtained by M_{codon}^{all} , which agrees with the codon chronology. The codons in (a) initial period, (b) transition period and (c) fulfilment period are in green, blue and red respectively. **b** The codon distance matrix M_{codon}^{all} and its averaging curve *Barrier*. There was a midway high “barrier” (*Barrier* \approx 0.5) in the genetic code evolution between the initial period and the fulfilment period. **c** The phylogenetic tree of eukaryotes obtained by their codon interval distance matrix M_{ci}^{euk} .

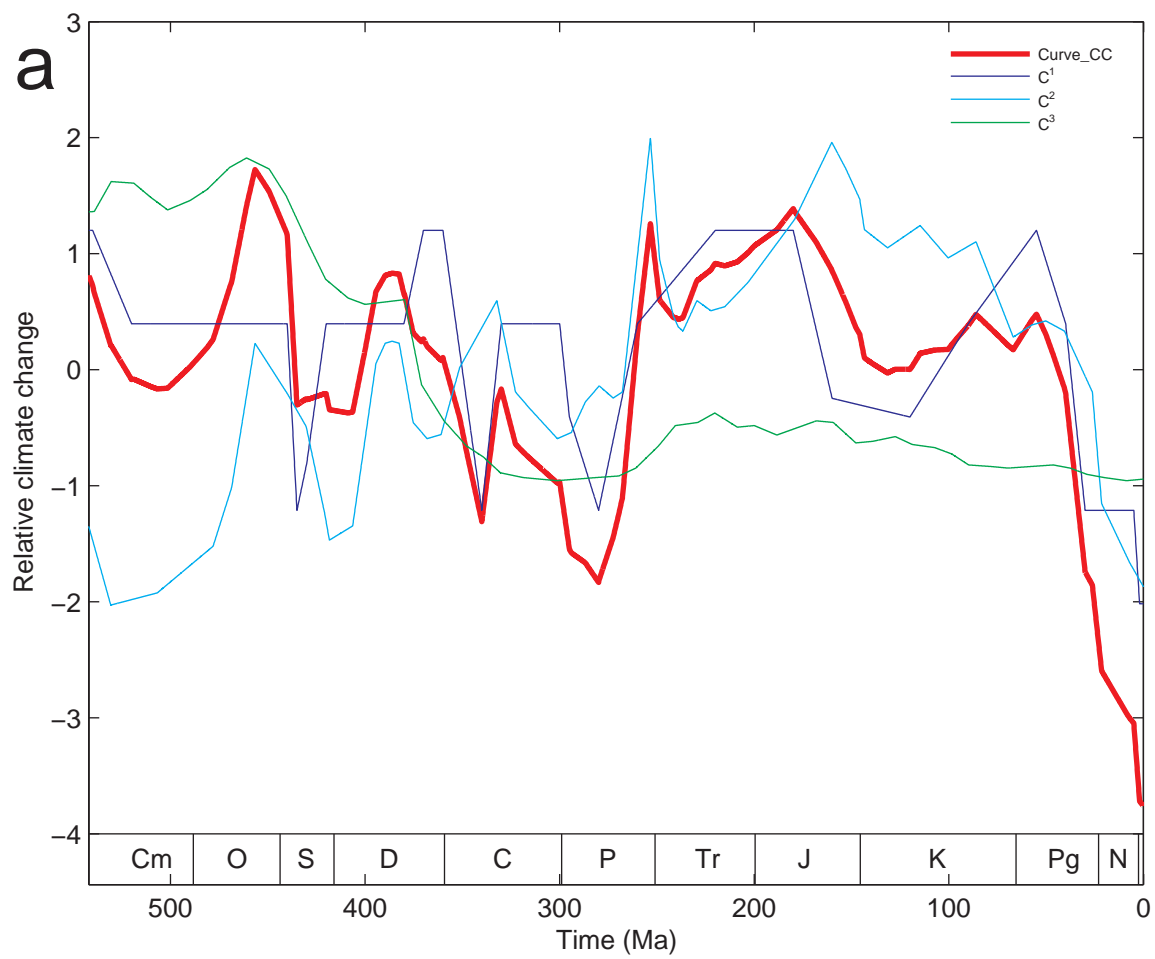


Figure 5: **Fig. S1a** The climate curves.

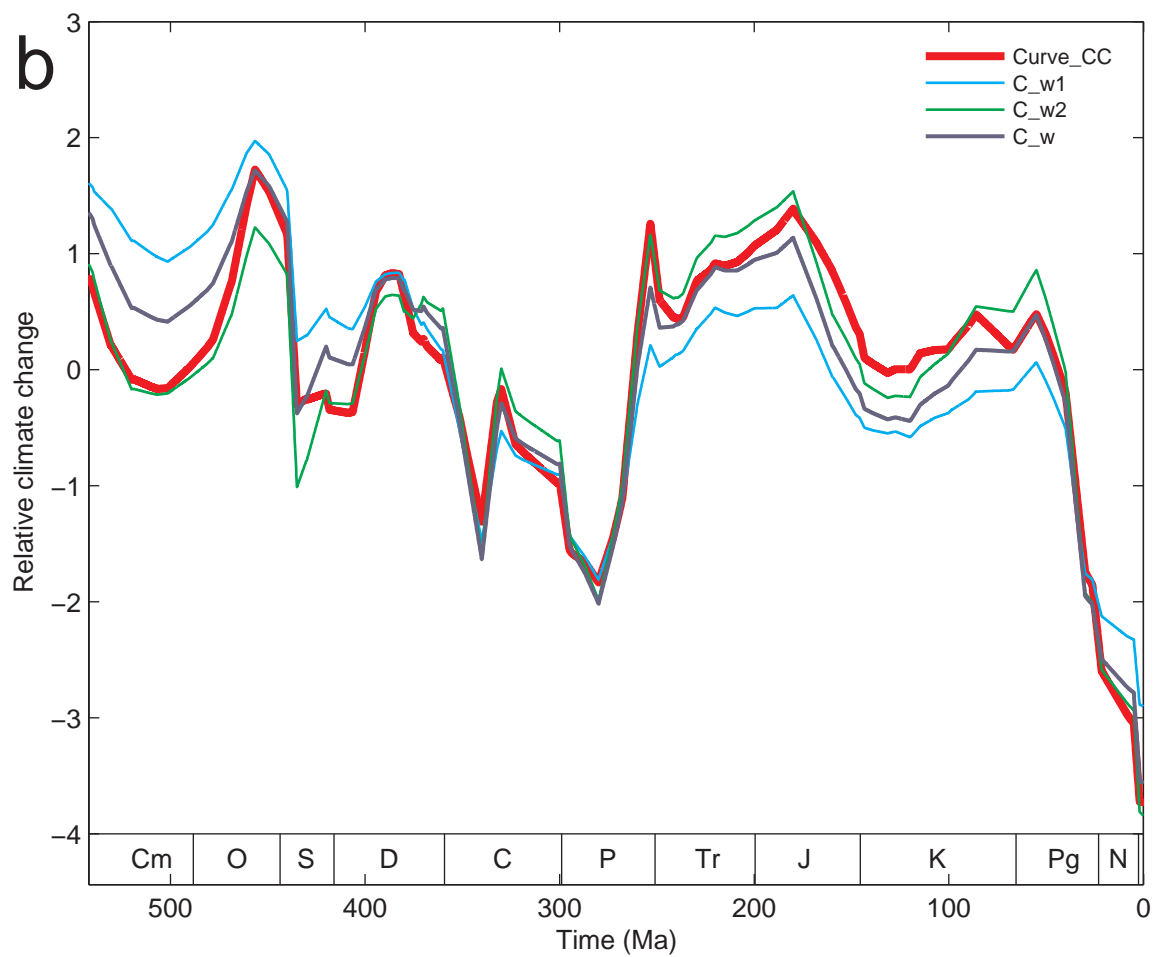


Figure 6: **Fig. S1b** The error range of *Curve_CC*.

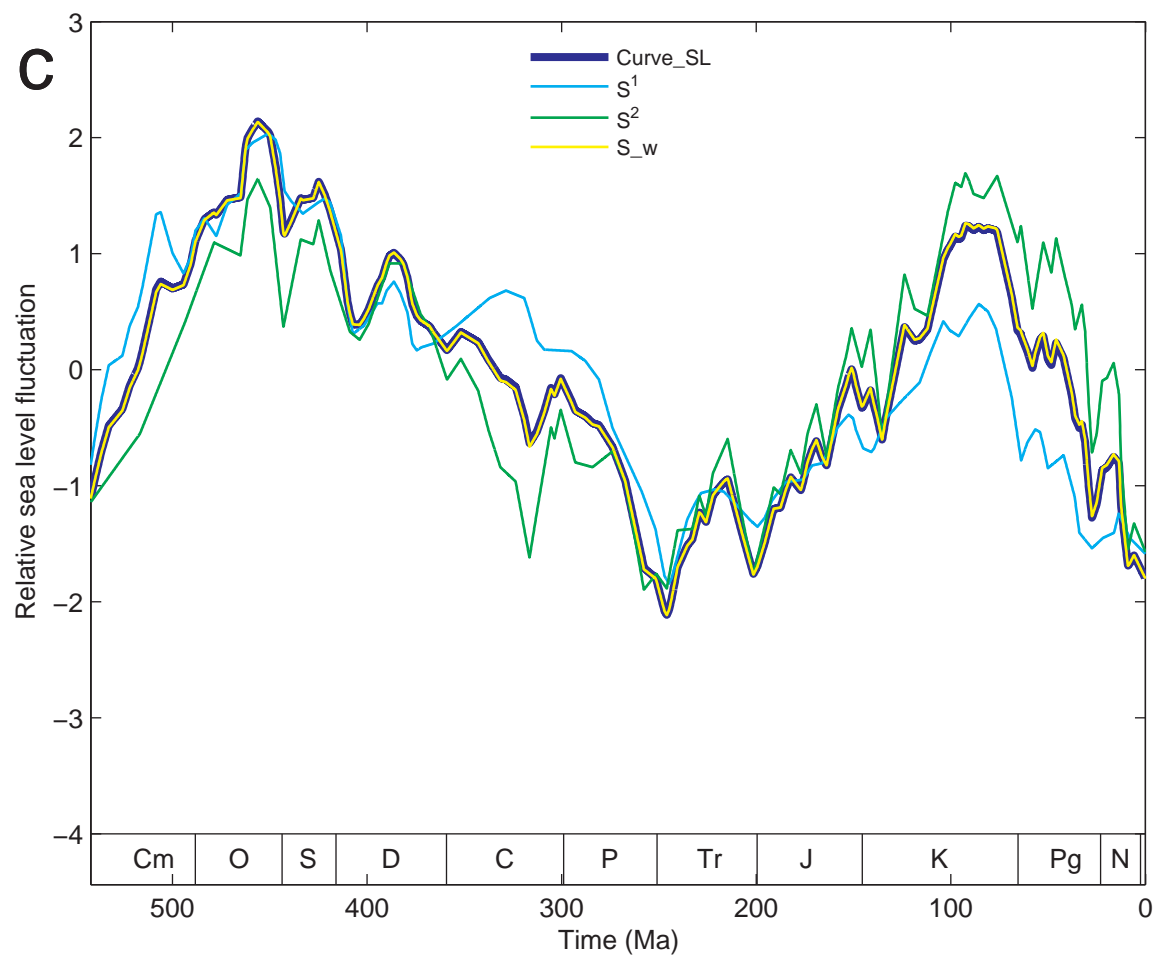


Figure 7: **Fig. S1c** The error range of *Curve_SL*.

d

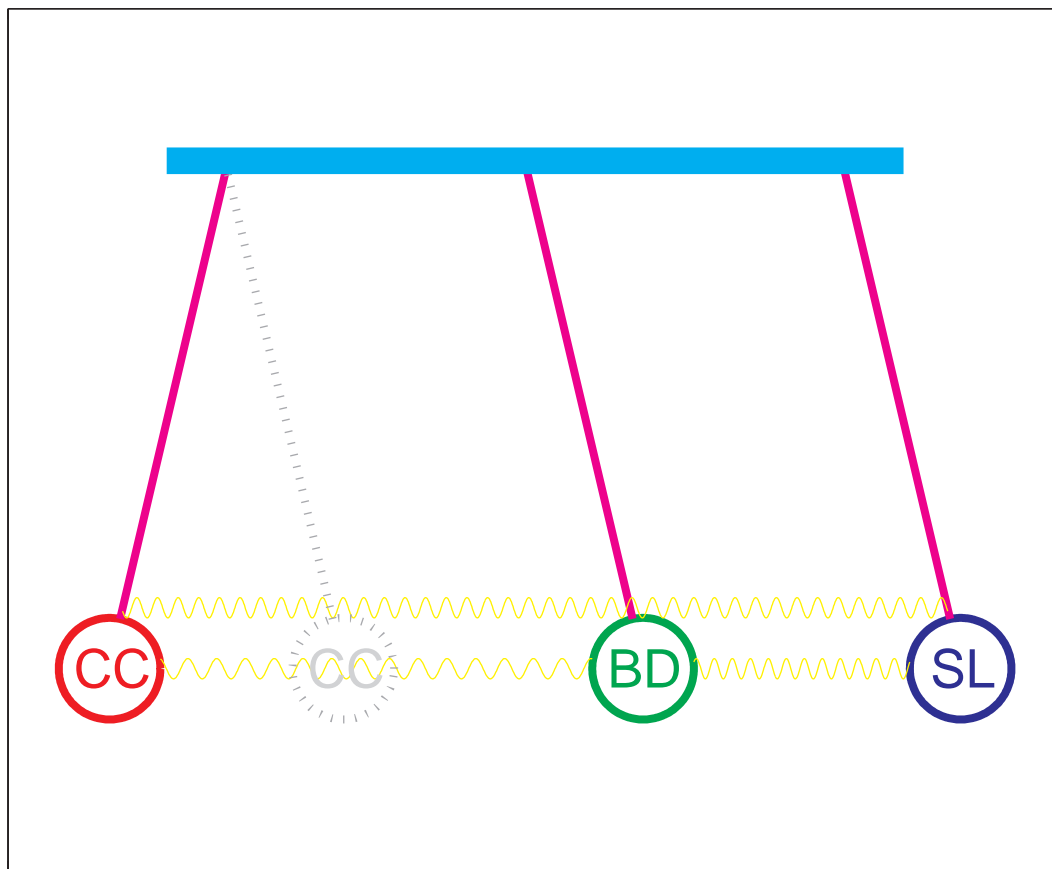


Figure 8: **Fig. S1d** Simulating climate phase reverse by a triple pendulum model.

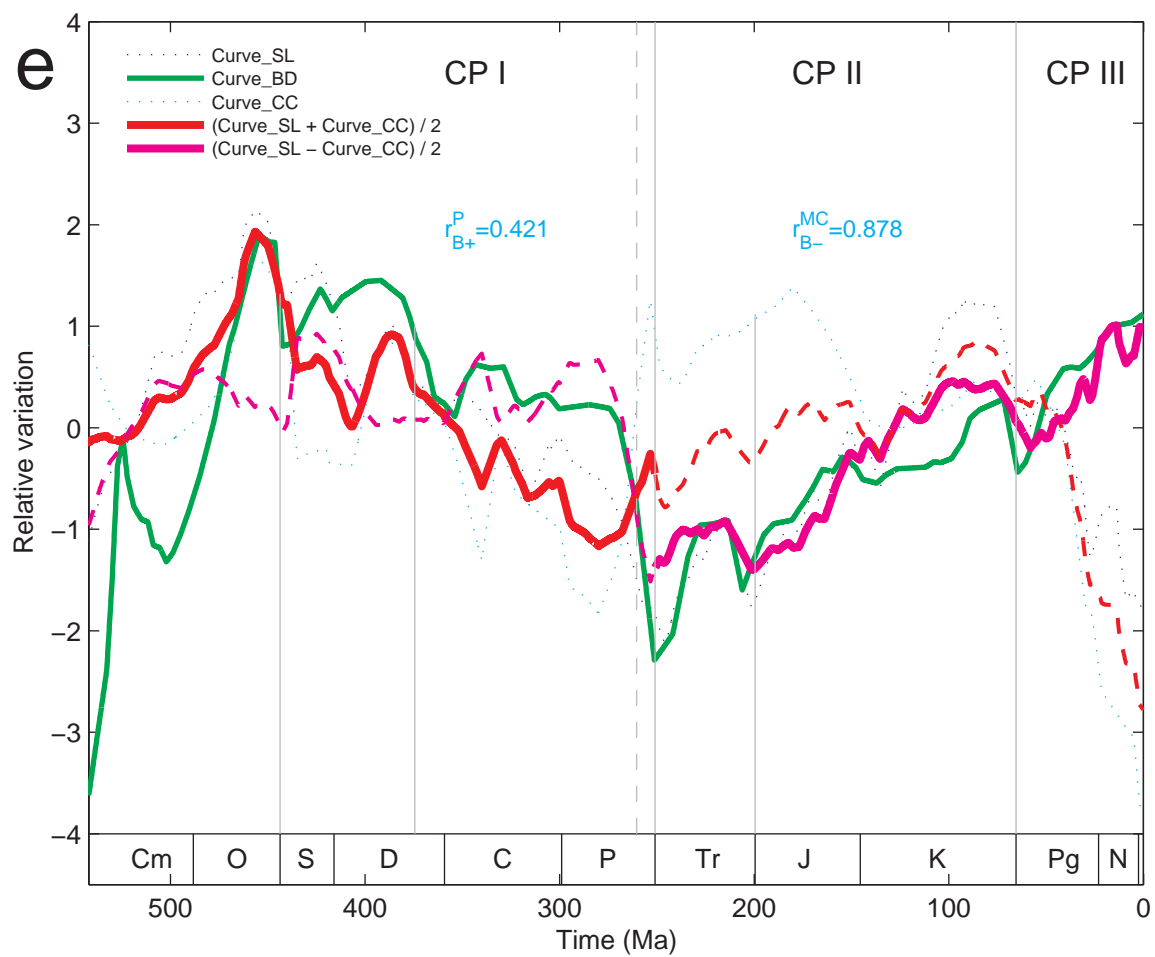


Figure 9: **Fig. S1e** The tectonic curve.

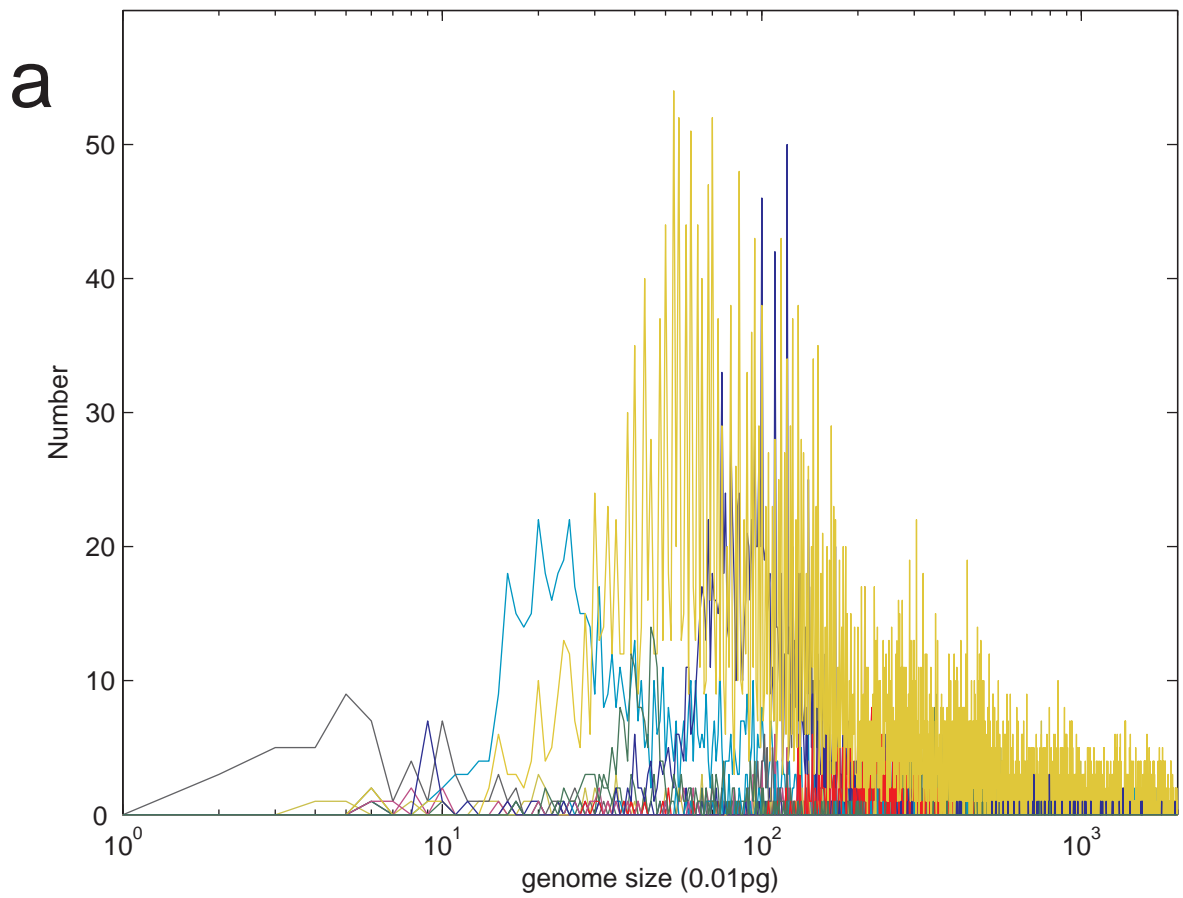


Figure 10: **Fig. S2a** Log-normal distributions of genome sizes in taxa.

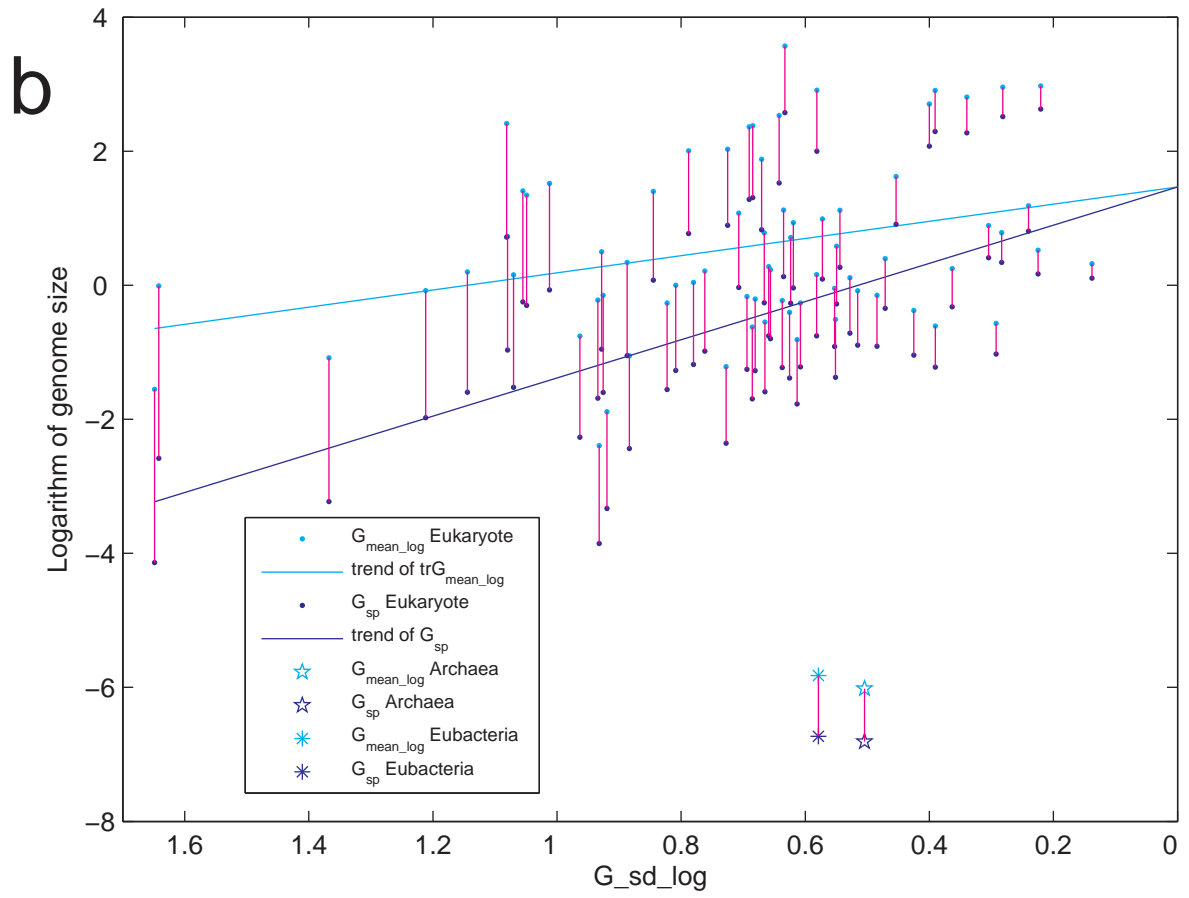


Figure 11: **Fig. S2b** G_{sd_log} tends to decline with respect to G_{sp} .

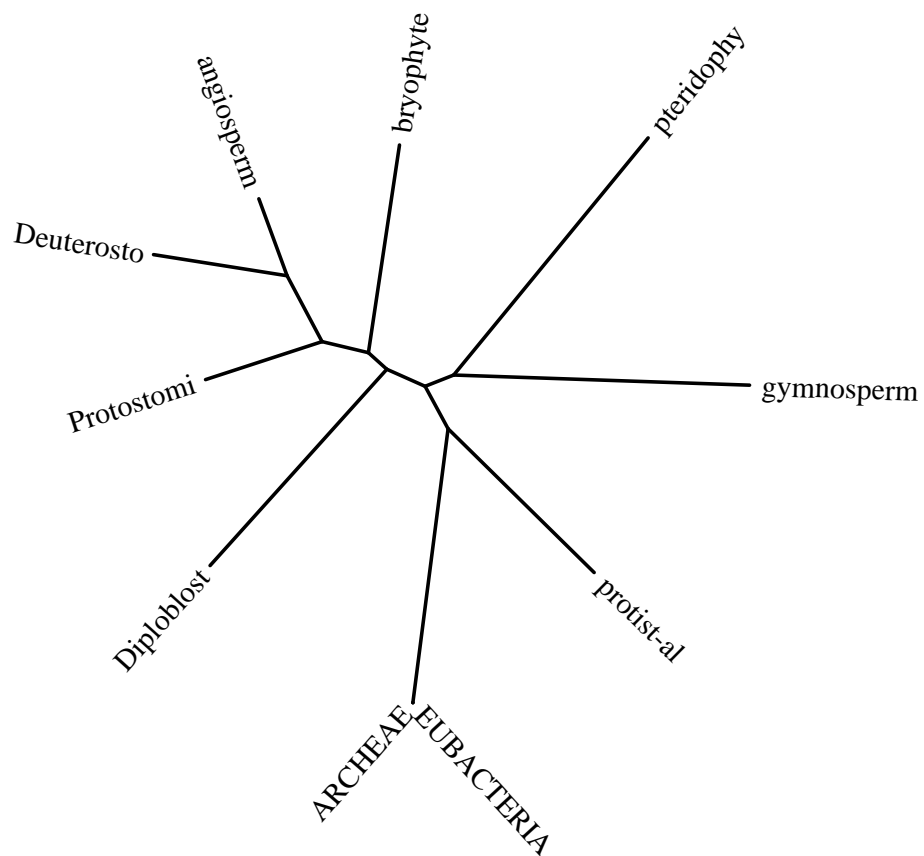


Figure 12: **Fig. S2c** The phylogenetic tree based on M_{gs}^P .

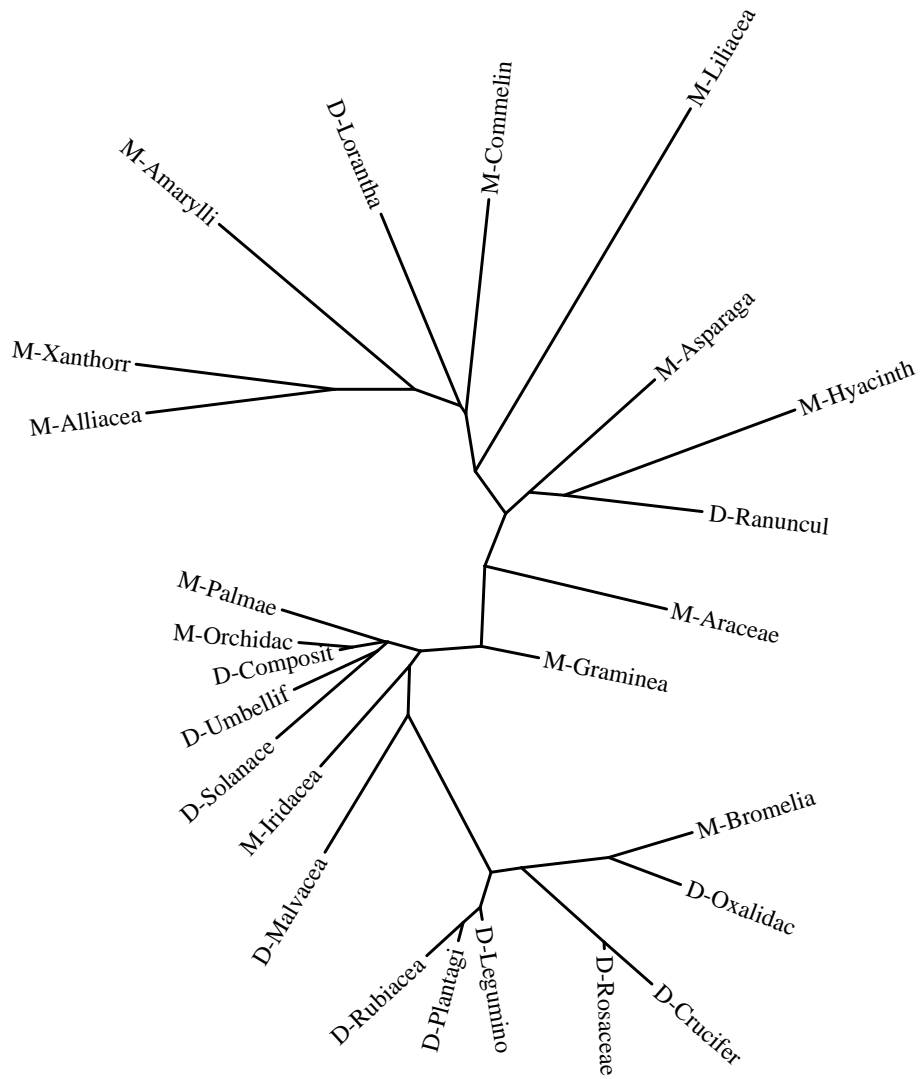
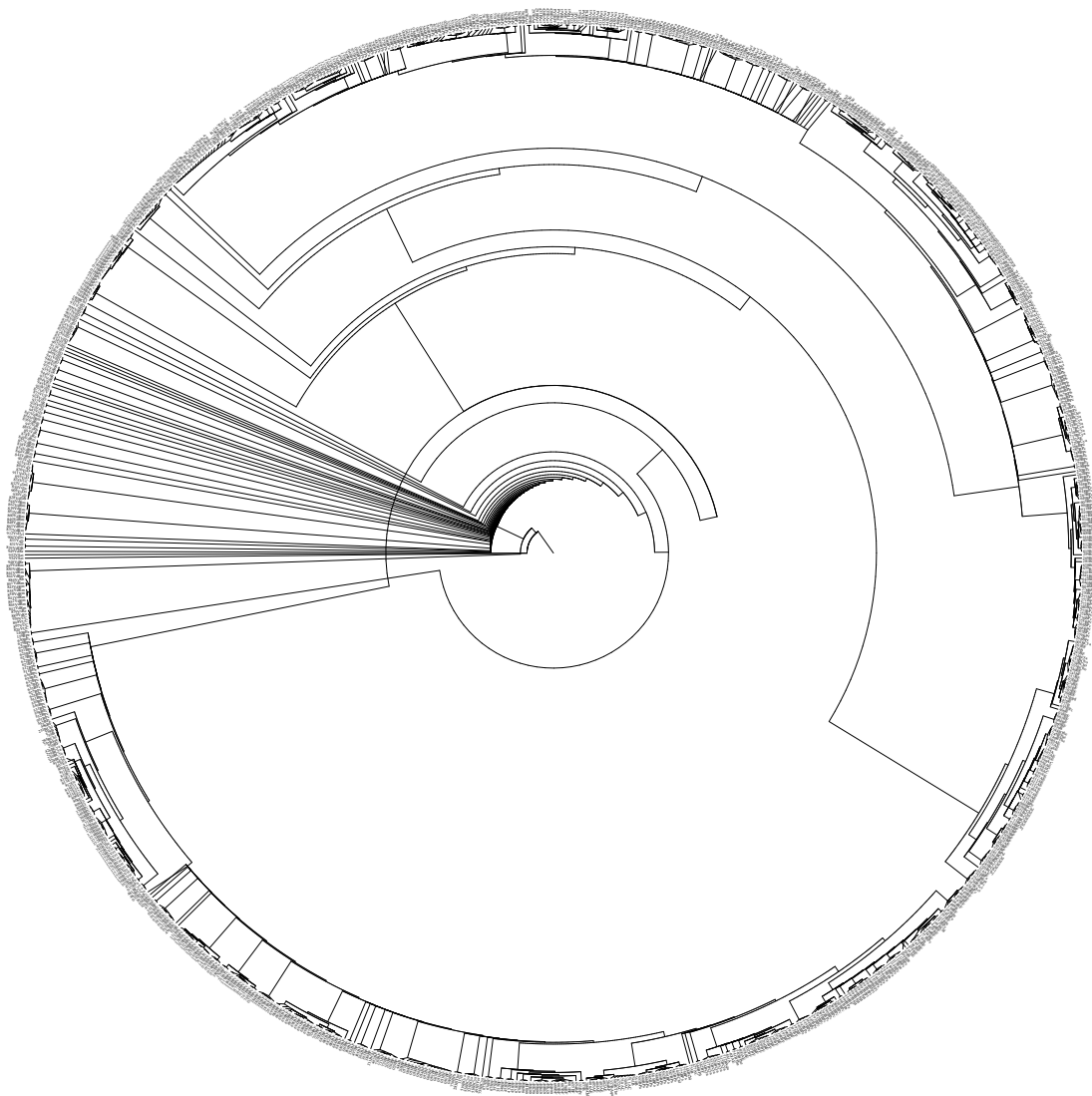


Figure 13: **Fig. S2d** The phylogenetic tree based on $M_{gs}^{angiosperm}$.



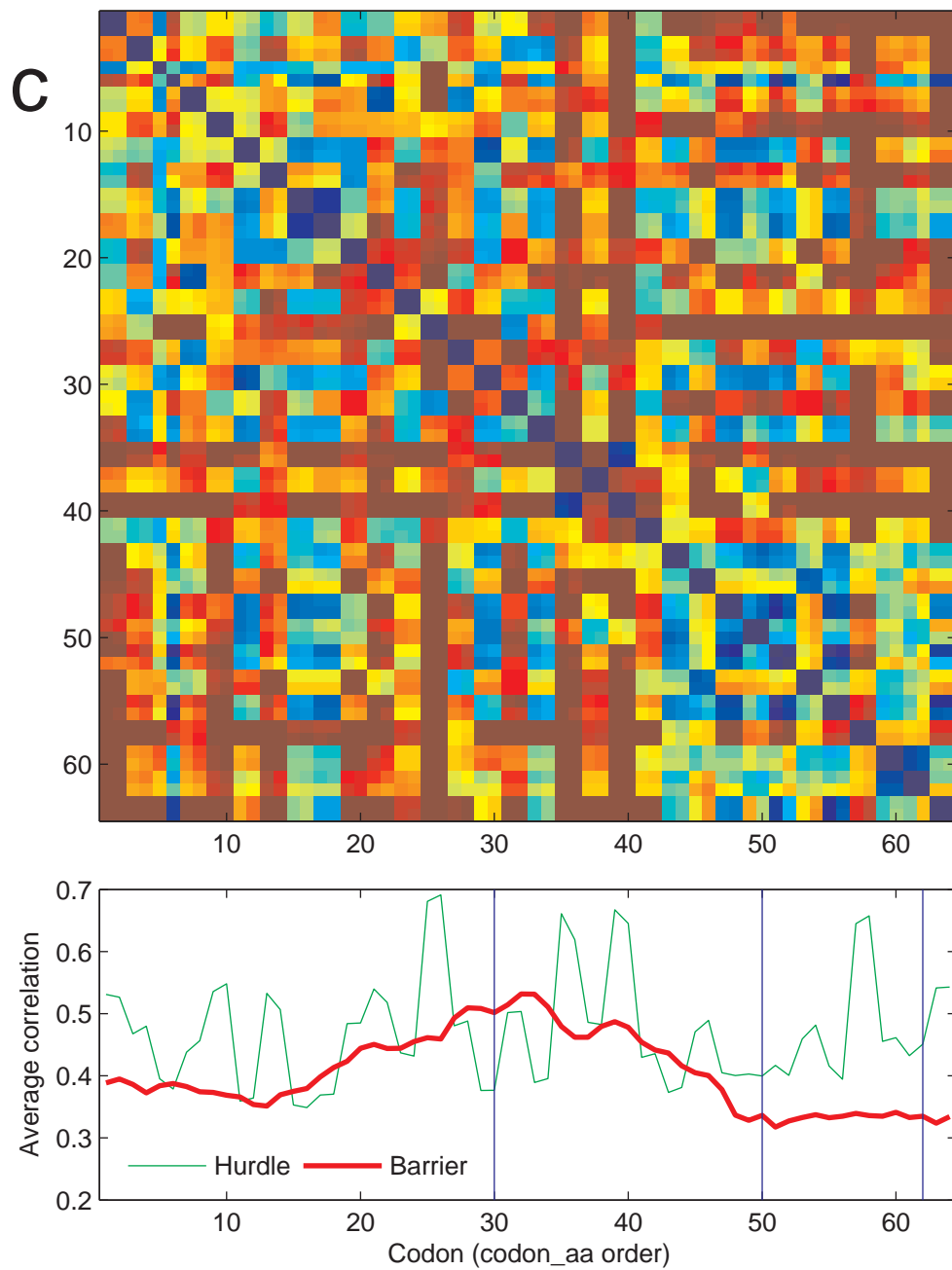


Figure 16: **Fig. S3c** The correlation matrix M_{codon}^{euk} and Curve *Barrier*.

Table 1: **Correlation coefficients** $r_{\mu\nu}^\rho$

n		$r_{\mu\nu}^p$	P	M	C	PMC	PM	MC	$P \setminus L$	L	$L.M.Tr$	$M \setminus L.M.Tr$	R^+	R^-	ΔR	Q	Q'	ΔQ
1	$Curve_{\mathcal{S}L}$	SB	0.593	0.905	-0.831	0.564	0.703	0.390	0.536	0.923	0.957	0.915	0.516	-0.611	1.126	0.545	0.343	0.202
	$Curve_{BD}$	BC	0.114	-0.431	-0.881	-0.287	-0.161	-0.752	0.196	-0.901	0.205	-0.638						
	$Curve_{CC}$	CS	0.494	-0.617	0.950	0.217	0.003	0.108	0.658	-0.904	0.248	-0.726						
2	$Curve_{\mathcal{S}L}$	SB	0.593	0.905	-0.831	0.564	0.703	0.390	0.536	0.923	0.957	0.915	0.308	-0.583	0.891	0.477	0.370	0.106
	$Curve_{BD}$	BC^1	-0.233	-0.470	-0.887	-0.399	-0.339	-0.659	-0.219	-0.999	0.980	-0.518						
	C^1	C^1S	0.043	-0.502	0.934	-0.006	-0.251	-0.023	0.086	-0.929	0.938	-0.485						
3	$Curve_{\mathcal{S}L}$	SB	0.593	0.905	-0.831	0.564	0.703	0.390	0.536	0.923	0.957	0.915	0.378	-0.038	0.416	0.469	0.372	0.097
	$Curve_{BD}$	BC^2	0.335	0.310	-0.804	-0.185	-0.131	-0.561	0.572	-0.827	-0.593	0.148						
	C^2	C^2S	-0.246	0.165	0.891	-0.236	-0.359	0.300	-0.063	-0.857	-0.537	-0.009						
4	$Curve_{\mathcal{S}L}$	SB	0.593	0.905	-0.831	0.564	0.703	0.390	0.536	0.923	0.957	0.915	0.525	-0.748	1.273	0.605	0.458	0.147
	$Curve_{BD}$	BC^3	-0.031	-0.627	-0.820	0.095	0.180	-0.821	-0.098	-1.000	0.837	-0.805						
	C^3	C^3S	0.677	-0.815	0.940	0.564	0.549	-0.379	0.669	-0.922	0.809	-0.883						
5	$Curve_{\mathcal{S}L}$	SB	0.593	0.905	-0.831	0.564	0.703	0.390	0.536	0.923	0.957	0.915	0.509	-0.691	1.200	0.575	0.373	0.202
	$Curve_{BD}$	BC_{w1}	-0.027	-0.564	-0.888	-0.158	-0.011	-0.784	-0.042	-0.949	0.965	-0.711						
	C_{w1}	$C_{w1}S$	0.609	-0.700	0.951	0.433	0.333	0.003	0.652	-0.930	0.953	-0.748						
6	$Curve_{\mathcal{S}L}$	SB	0.593	0.905	-0.831	0.564	0.703	0.390	0.536	0.923	0.957	0.915	0.454	-0.621	1.075	0.506	0.366	0.139
	$Curve_{BD}$	BC_{w2}	0.027	-0.474	-0.889	-0.353	-0.262	-0.746	0.111	-0.915	0.621	-0.616						
	C_{w2}	$C_{w2}S$	0.344	-0.599	0.951	0.115	0.149	0.079	0.503	-0.913	0.638	-0.652						
7	$Curve_{\mathcal{S}L}$	SB	0.593	0.905	-0.831	0.564	0.703	0.390	0.536	0.923	0.957	0.915	0.494	-0.654	1.148	0.545	0.361	0.184
	$Curve_{BD}$	BC_w	-0.006	-0.517	-0.889	-0.267	-0.135	-0.763	0.018	-0.931	0.842	-0.661						
	C_w	C_wS	0.529	-0.647	0.951	0.299	0.131	0.047	0.617	-0.921	0.845	-0.697						
8	S^1	S^1B	0.506	0.901	-0.848	0.481	0.687	0.182	0.431	0.998	0.928	0.888	0.471	-0.601	1.072	0.511	0.337	0.174
	$Curve_{BD}$	BC	0.114	-0.431	-0.881	-0.287	-0.161	-0.752	0.196	-0.901	0.205	-0.638						
	$Curve_{CC}$	CS^1	0.420	-0.586	0.915	0.182	-0.132	0.274	0.584	-0.878	0.436	-0.709						
9	S^2	S^2B	0.613	0.894	-0.776	0.530	0.611	0.489	0.566	0.039	0.906	0.915	0.521	-0.607	1.128	0.548	0.341	0.207
	$Curve_{BD}$	BC	0.114	-0.431	-0.881	-0.287	-0.161	-0.752	0.196	-0.901	0.205	-0.638						
	$Curve_{CC}$	CS^2	0.513	-0.627	0.909	0.207	0.131	0.001	0.650	-0.258	0.030	-0.724						
10	S_w	S_wB	0.594	0.905	-0.830	0.565	0.702	0.393	0.538	0.915	0.957	0.915	0.516	-0.611	1.127	0.545	0.343	0.202
	$Curve_{BD}$	BC	0.114	-0.431	-0.881	-0.287	-0.161	-0.752	0.196	-0.901	0.205	-0.638						
	$Curve_{CC}$	CS_w	0.495	-0.618	0.949	0.217	0.007	0.105	0.659	-0.902	0.243	-0.726						

Table 2: **Metazoan origination** ($G_{sp} = G_{mean_log} - \chi \cdot G_{sd_log}$, $\chi = 1.5677$)

No.	Superphylum	Taxon	number of records	G_{mean_log}	G_{sd_log}	G_{sp}	T_{ori} (Ma)
1	Protostomia	Nematodes	66	-2.394	0.93204	-3.8552	572.89
2	Deuterostomia	Chordates	5	-1.8885	0.91958	-3.3301	566.49
3	Diploblostica	Sponges	7	-1.0834	1.3675	-3.2272	565.23
4	Diploblostica	Ctenophores	2	-0.010305	1.6417	-2.584	557.39
5	Protostomia	Tardigrades	21	-1.2168	0.7276	-2.3574	554.63
6	Protostomia	Misc_Inverts	57	-0.75852	0.96321	-2.2686	553.54
7	Protostomia	Arthropod	1284	-0.078413	1.2116	-1.9778	550
8	Protostomia	Annelid	140	-0.14875	0.9258	-1.6001	545.39
9	Protostomia	Myriapods	15	-0.54874	0.66478	-1.5909	545.28
10	Protostomia	Flatworms	68	0.15556	1.0701	-1.522	544.44
11	Protostomia	Rotifers	9	-0.51158	0.55134	-1.3759	542.66
12	Diploblostica	Cnidarians	11	-0.16888	0.69379	-1.2565	541.2
13	Deuterostomia	Fish	2045	0.23067	0.6559	-0.7976	535.6
14	Deuterostomia	Echinoderm	48	0.11223	0.52794	-0.71542	534.6
15	Protostomia	Molluscs	263	0.5812	0.5493	-0.27994	529.29
16	Deuterostomia	Bird	474	0.32019	0.13788	0.10403	524.61
17	Deuterostomia	Reptile	418	0.78332	0.28332	0.33916	521.74
18	Deuterostomia	Amphibian	927	2.4116	1.081	0.71691	517.13
19	Deuterostomia	Mammal	657	1.1837	0.2401	0.80727	516.03

Table 3: **Metazoan origination** ($G'_{sp} = G_{mean_log} - \chi_1 \cdot G_{sd_log}$, $\chi_1 = 3.1867$)

No.	Superphylum	Taxon	number of records	G_{mean_log}	G_{sd_log}	G_{sp}	$G_{sp}' (\chi_1)$	T_{ori} (Ma)
3	Diploblostica	Sponges	7	-1.0834	1.3675	-3.2272	-5.4412	565.23
1	Protostomia	Nematodes	66	-2.394	0.93204	-3.8552	-5.3641	572.89
4	Diploblostica	Ctenophores	2	-0.010305	1.6417	-2.584	-5.2419	557.39
2	Deuterostomia	Chordates	5	-1.8885	0.91958	-3.3301	-4.8189	566.49
7	Protostomia	Arthropod	1284	-0.078413	1.2116	-1.9778	-3.9394	550
6	Protostomia	Misc_Inverts	57	-0.75852	0.96321	-2.2686	-3.828	553.54
5	Protostomia	Tardigrades	21	-1.2168	0.7276	-2.3574	-3.5354	554.63
10	Protostomia	Flatworms	68	0.15556	1.0701	-1.522	-3.2545	544.44
8	Protostomia	Annelid	140	-0.14875	0.9258	-1.6001	-3.099	545.39
9	Protostomia	Myriapods	15	-0.54874	0.66478	-1.5909	-2.6672	545.28
12	Diploblostica	Cnidarians	11	-0.16888	0.69379	-1.2565	-2.3798	541.2
11	Protostomia	Rotifers	9	-0.51158	0.55134	-1.3759	-2.2685	542.66
13	Deuterostomia	Fish	2045	0.23067	0.6559	-0.7976	-1.8595	535.6
14	Deuterostomia	Echinoderm	48	0.11223	0.52794	-0.7154	-1.5702	534.6
15	Protostomia	Molluscs	263	0.5812	0.5493	-0.2799	-1.1693	529.29
18	Deuterostomia	Amphibian	927	2.4116	1.081	0.71691	-1.0332	517.13
17	Deuterostomia	Reptile	418	0.78332	0.28332	0.33916	-0.1195	521.74
16	Deuterostomia	Bird	474	0.32019	0.13788	0.10403	-0.1192	524.61
19	Deuterostomia	Mammal	657	1.1837	0.2401	0.80727	0.41857	516.03

Table 4: Metazoan origination (G_{mean_log})

No.	Superphylum	Taxon	number of records	G_{mean_log}	G_{sd_log}	G_{sp}	T_{ori} (Ma)
1	Protostomia	Nematodes	66	-2.394	0.93204	-3.8552	572.89
2	Deuterostomia	Chordates	5	-1.8885	0.91958	-3.3301	566.49
5	Protostomia	Tardigrades	21	-1.2168	0.7276	-2.3574	554.63
3	Diploblostica	Sponges	7	-1.0834	1.3675	-3.2272	565.23
6	Protostomia	Misc.Inverts	57	-0.75852	0.96321	-2.2686	553.54
9	Protostomia	Myriapods	15	-0.54874	0.66478	-1.5909	545.28
11	Protostomia	Rotifers	9	-0.51158	0.55134	-1.3759	542.66
12	Diploblostica	Cnidarians	11	-0.16888	0.69379	-1.2565	541.2
8	Protostomia	Annelid	140	-0.14875	0.9258	-1.6001	545.39
7	Protostomia	Arthropod	1284	-0.078413	1.2116	-1.9778	550
4	Diploblostica	Ctenophores	2	-0.010305	1.6417	-2.584	557.39
14	Deuterostomia	Echinoderm	48	0.11223	0.52794	-0.71542	534.6
10	Protostomia	Flatworms	68	0.15556	1.0701	-1.522	544.44
13	Deuterostomia	Fish	2045	0.23067	0.6559	-0.7976	535.6
16	Deuterostomia	Bird	474	0.32019	0.13788	0.10403	524.61
15	Protostomia	Molluscs	263	0.5812	0.5493	-0.27994	529.29
17	Deuterostomia	Reptile	418	0.78332	0.28332	0.33916	521.74
19	Deuterostomia	Mammal	657	1.1837	0.2401	0.80727	516.03
18	Deuterostomia	Amphibian	927	2.4116	1.081	0.71691	517.13

Table 5: **Angiosperm origination** ($G_{sp} = G_{mean_log} - \chi \cdot G_{sd_log}$, $\chi = 1.5677$)

No.	Superphylum	Taxon	G_{mean_log}	G_{sd_log}	G_{sp}	T_{ori} (Ma)
1	Dicotyledoneae	Lentibulariaceae	-1.0532	0.88349	-2.4382	177.96
2	Monocotyledoneae	Cyperaceae	-0.81211	0.61307	-1.7732	169.85
3	Dicotyledoneae	Cruciferae	-0.62192	0.6855	-1.6966	168.91
4	Dicotyledoneae	Rutaceae	-0.22121	0.93413	-1.6856	168.78
5	Dicotyledoneae	Oxalidaceae	0.19774	1.1445	-1.5964	167.69
6	Dicotyledoneae	Crassulaceae	-0.26578	0.82268	-1.5555	167.19
7	Dicotyledoneae	Rosaceae	-0.40468	0.62511	-1.3847	165.11
8	Dicotyledoneae	Boraginaceae	-0.20664	0.68081	-1.2739	163.76
9	Dicotyledoneae	Labiatae	-0.0021905	0.80883	-1.2702	163.71
10	Monocotyledoneae	Juncaceae	-0.23032	0.63698	-1.2289	163.21
11	Dicotyledoneae	Vitaceae	-0.60987	0.39049	-1.222	163.13
12	Dicotyledoneae	Cucurbitaceae	-0.26487	0.60779	-1.2177	163.07
13	Dicotyledoneae	Onagraceae	0.040848	0.78018	-1.1822	162.64
14	Dicotyledoneae	Leguminosae	0.33968	0.88684	-1.0506	161.04
15	Dicotyledoneae	Myrtaceae	-0.37801	0.42511	-1.0445	160.96
16	Monocotyledoneae	Bromeliaceae	-0.56838	0.29232	-1.0266	160.74
17	Dicotyledoneae	Polygonaceae	0.20985	0.76174	-0.98433	160.23
18	Dicotyledoneae	Euphorbiaceae	0.72687	1.0796	-0.96561	160
19	Dicotyledoneae	Convolvulaceae	0.50052	0.928	-0.9543	159.86
20	Dicotyledoneae	Chenopodiaceae	-0.046809	0.5526	-0.91312	159.36
21	Dicotyledoneae	Plantaginaceae	-0.15021	0.48422	-0.90932	159.31
22	Dicotyledoneae	Rubiaceae	-0.084413	0.51565	-0.8928	159.11
23	Dicotyledoneae	Caryophyllaceae	0.27683	0.65869	-0.7558	157.44
24	Dicotyledoneae	Amaranthaceae	0.15834	0.58176	-0.75369	157.42
25	Dicotyledoneae	Malvaceae	0.39517	0.47109	-0.34336	152.41
26	Monocotyledoneae	Zingiberaceae	0.24819	0.36317	-0.32115	152.14
27	Monocotyledoneae	Iridaceae	1.3429	1.0491	-0.30178	151.9
28	Dicotyledoneae	Umbelliferae	0.71003	0.6235	-0.26742	151.49
29	Dicotyledoneae	Solanaceae	0.78034	0.66585	-0.26352	151.44
30	Monocotyledoneae	Orchidaceae	1.4063	1.0551	-0.24784	151.25
31	Monocotyledoneae	Araceae	1.5174	1.012	-0.069152	149.07
32	Dicotyledoneae	Papaveraceae	0.93206	0.61932	-0.038854	148.7
33	Dicotyledoneae	Compositae	1.0741	0.70726	-0.034657	148.65
34	Monocotyledoneae	Gramineae	1.4002	0.84476	0.075894	147.3
35	Dicotyledoneae	Cactaceae	0.98813	0.57251	0.090608	147.12
36	Monocotyledoneae	Palmae	1.1222	0.63488	0.12691	146.68
37	Dicotyledoneae	Passifloraceae	0.52209	0.22472	0.16979	146.15
38	Dicotyledoneae	Orobanchaceae	1.12	0.54393	0.26726	144.97
39	Dicotyledoneae	Cistaceae	0.88905	0.30458	0.41155	143.21
40	Monocotyledoneae	Asparagaceae	2.0053	0.78802	0.76991	138.84
41	Dicotyledoneae	Asteraceae	1.8795	0.67031	0.82863	138.12
42	Dicotyledoneae	Ranunculaceae	2.0285	0.72517	0.8916	137.35
43	Monocotyledoneae	Agavaceae	1.6207	0.4537	0.90941	137.13
44	Monocotyledoneae	Hyacinthaceae	2.3635	0.69028	1.2814	132.6
45	Dicotyledoneae	Loranthaceae	2.3797	0.68478	1.3062	132.3
46	Monocotyledoneae	Commelinaceae	2.5322	0.64196	1.5258	129.62
47	Monocotyledoneae	Amaryllidaceae	2.9085	0.5811	1.9975	123.86
48	Monocotyledoneae	Xanthorrhoeaceae	2.7036	0.4	2.0765	122.9
49	Monocotyledoneae	Asphodelaceae	2.8054	0.33968	2.2729	120.51
50	Monocotyledoneae	Alliaceae	2.9051	0.39078	2.2924	120.27
51	Dicotyledoneae	Paeoniaceae	2.957	0.28164	2.5155	117.55
52	Monocotyledoneae	Liliaceae	3.5678	0.63278	2.5757	116.81
53	Monocotyledoneae	Aloaceae	2.9724	0.2203	2.627	116.19

Table 6: Angiosperm origination ($G'_{sp} = G_{mean_log} - \chi_1 \cdot G_{sd_log}$, $\chi_1 = 3.1867$)

No.	Superphylum	Taxon	G_{mean_log}	G_{sd_log}	G_{sp}	G'_{sp}	T_{ori} (Ma)
1	Dicotyledoneae	Lentibulariaceae	-1.0532	0.88349	-2.4382	-3.8686	177.96
5	Dicotyledoneae	Oxalidaceae	0.19774	1.1445	-1.5964	-3.4494	167.69
4	Dicotyledoneae	Rutaceae	-0.22121	0.93413	-1.6856	-3.198	168.78
6	Dicotyledoneae	Crassulaceae	-0.26578	0.82268	-1.5555	-2.8874	167.19
3	Dicotyledoneae	Cruciferae	-0.62192	0.6855	-1.6966	-2.8064	168.91
2	Monocotyledoneae	Cyperaceae	-0.81211	0.61307	-1.7732	-2.7658	169.85
18	Dicotyledoneae	Euphorbiaceae	0.72687	1.0796	-0.96561	-2.7135	160
9	Dicotyledoneae	Labiatae	-0.0021905	0.80883	-1.2702	-2.5797	163.71
14	Dicotyledoneae	Leguminosae	0.33968	0.88684	-1.0506	-2.4864	161.04
19	Dicotyledoneae	Convolvulaceae	0.50052	0.928	-0.9543	-2.4567	159.86
13	Dicotyledoneae	Onagraceae	0.040848	0.78018	-1.1822	-2.4454	162.64
7	Dicotyledoneae	Rosaceae	-0.40468	0.62511	-1.3847	-2.3967	165.11
8	Dicotyledoneae	Boraginaceae	-0.20664	0.68081	-1.2739	-2.3762	163.76
10	Monocotyledoneae	Juncaceae	-0.23032	0.63698	-1.2289	-2.2602	163.21
17	Dicotyledoneae	Polygonaceae	0.20985	0.76174	-0.98433	-2.2176	160.23
12	Dicotyledoneae	Cucurbitaceae	-0.26487	0.60779	-1.2177	-2.2017	163.07
27	Monocotyledoneae	Iridaceae	1.3429	1.0491	-0.30178	-2.0003	151.9
30	Monocotyledoneae	Orchidaceae	1.4063	1.0551	-0.24784	-1.956	151.25
11	Dicotyledoneae	Vitaceae	-0.60987	0.39049	-1.222	-1.8542	163.13
23	Dicotyledoneae	Caryophyllaceae	0.27683	0.65869	-0.7558	-1.8222	157.44
20	Dicotyledoneae	Chenopodiaceae	-0.046809	0.5526	-0.91312	-1.8078	159.36
15	Dicotyledoneae	Myrtaceae	-0.37801	0.42511	-1.0445	-1.7327	160.96
22	Dicotyledoneae	Rubiaceae	-0.084413	0.51565	-0.8928	-1.7276	159.11
31	Monocotyledoneae	Araceae	1.5174	1.012	-0.069152	-1.7075	149.07
24	Dicotyledoneae	Amaranthaceae	0.15834	0.58176	-0.75369	-1.6956	157.42
21	Dicotyledoneae	Plantaginaceae	-0.15021	0.48422	-0.90932	-1.6933	159.31
16	Monocotyledoneae	Bromeliaceae	-0.56838	0.29232	-1.0266	-1.4999	160.74
29	Dicotyledoneae	Solanaceae	0.78034	0.66585	-0.26352	-1.3415	151.44
34	Monocotyledoneae	Gramineae	1.4002	0.84476	0.075894	-1.2918	147.3
28	Dicotyledoneae	Umbelliferae	0.71003	0.6235	-0.26742	-1.2769	151.49
33	Dicotyledoneae	Compositae	1.0741	0.70726	-0.034657	-1.1797	148.65
25	Dicotyledoneae	Malvaceae	0.39517	0.47109	-0.34336	-1.1061	152.41
32	Dicotyledoneae	Papaveraceae	0.93206	0.61932	-0.038854	-1.0415	148.7
26	Monocotyledoneae	Zingiberaceae	0.24819	0.36317	-0.32115	-0.9091	152.14
36	Monocotyledoneae	Palmae	1.1222	0.63488	0.12691	-0.901	146.68
35	Dicotyledoneae	Cactaceae	0.98813	0.57251	0.090608	-0.8363	147.12
38	Dicotyledoneae	Orobanchaceae	1.12	0.54393	0.26726	-0.6133	144.97
40	Monocotyledoneae	Asparagaceae	2.0053	0.78802	0.76991	-0.5059	138.84
42	Dicotyledoneae	Ranunculaceae	2.0285	0.72517	0.8916	-0.2824	137.35
41	Dicotyledoneae	Asteraceae	1.8795	0.67031	0.82863	-0.2566	138.12
37	Dicotyledoneae	Passifloraceae	0.52209	0.22472	0.16979	-0.194	146.15
39	Dicotyledoneae	Cistaceae	0.88905	0.30458	0.41155	-0.0816	143.21
44	Monocotyledoneae	Hyacinthaceae	2.3635	0.69028	1.2814	0.16378	132.6
43	Monocotyledoneae	Agavaceae	1.6207	0.4537	0.90941	0.17489	137.13
45	Dicotyledoneae	Loranthaceae	2.3797	0.68478	1.3062	0.19751	132.3
46	Monocotyledoneae	Commelinaceae	2.5322	0.64196	1.5258	0.48647	129.62
47	Monocotyledoneae	Amaryllidaceae	2.9085	0.5811	1.9975	1.05671	123.86
48	Monocotyledoneae	Xanthorrhoeaceae	2.7036	0.4	2.0765	1.42892	122.9
52	Monocotyledoneae	Liliaceae	3.5678	0.63278	2.5757	1.55132	116.81
50	Monocotyledoneae	Alliaceae	2.9051	0.39078	2.2924	1.6598	120.27
49	Monocotyledoneae	Asphodelaceae	2.8054	0.33968	2.2729	1.72294	120.51
51	Dicotyledoneae	Paoniaceae	2.957	0.28164	2.5155	2.0595	117.55
53	Monocotyledoneae	Aloaceae	2.9724	0.2203	2.627	2.27037	116.19

Table 7: Angiosperm origination (G_{mean_log})

No.	Superphylum	Taxon	G_{mean_log}	G_{sd_log}	G_{sp}	T_{ori} (Ma)
1	Dicotyledoneae	Lentibulariaceae	-1.0532	0.88349	-2.4382	177.96
2	Monocotyledoneae	Cyperaceae	-0.81211	0.61307	-1.7732	169.85
3	Dicotyledoneae	Cruciferae	-0.62192	0.6855	-1.6966	168.91
11	Dicotyledoneae	Vitaceae	-0.60987	0.39049	-1.222	163.13
16	Monocotyledoneae	Bromeliaceae	-0.56838	0.29232	-1.0266	160.74
7	Dicotyledoneae	Rosaceae	-0.40468	0.62511	-1.3847	165.11
15	Dicotyledoneae	Myrtaceae	-0.37801	0.42511	-1.0445	160.96
6	Dicotyledoneae	Crassulaceae	-0.26578	0.82268	-1.5555	167.19
12	Dicotyledoneae	Cucurbitaceae	-0.26487	0.60779	-1.2177	163.07
10	Monocotyledoneae	Juncaceae	-0.23032	0.63698	-1.2289	163.21
4	Dicotyledoneae	Rutaceae	-0.22121	0.93413	-1.6856	168.78
8	Dicotyledoneae	Boraginaceae	-0.20664	0.68081	-1.2739	163.76
21	Dicotyledoneae	Plantaginaceae	-0.15021	0.48422	-0.90932	159.31
22	Dicotyledoneae	Rubiaceae	-0.084413	0.51565	-0.8928	159.11
20	Dicotyledoneae	Chenopodiaceae	-0.046809	0.5526	-0.91312	159.36
9	Dicotyledoneae	Labiatae	-0.0021905	0.80883	-1.2702	163.71
13	Dicotyledoneae	Onagraceae	0.040848	0.78018	-1.1822	162.64
24	Dicotyledoneae	Amaranthaceae	0.15834	0.58176	-0.75369	157.42
5	Dicotyledoneae	Oxalidaceae	0.19774	1.1445	-1.5964	167.69
17	Dicotyledoneae	Polygonaceae	0.20985	0.76174	-0.98433	160.23
26	Monocotyledoneae	Zingiberaceae	0.24819	0.36317	-0.32115	152.14
23	Dicotyledoneae	Caryophyllaceae	0.27683	0.65869	-0.7558	157.44
14	Dicotyledoneae	Leguminosae	0.33968	0.88684	-1.0506	161.04
25	Dicotyledoneae	Malvaceae	0.39517	0.47109	-0.34336	152.41
19	Dicotyledoneae	Convolvulaceae	0.50052	0.928	-0.9543	159.86
37	Dicotyledoneae	Passifloraceae	0.52209	0.22472	0.16979	146.15
28	Dicotyledoneae	Umbelliferae	0.71003	0.6235	-0.26742	151.49
18	Dicotyledoneae	Euphorbiaceae	0.72687	1.0796	-0.96561	160
29	Dicotyledoneae	Solanaceae	0.78034	0.66585	-0.26352	151.44
39	Dicotyledoneae	Cistaceae	0.88905	0.30458	0.41155	143.21
32	Dicotyledoneae	Papaveraceae	0.93206	0.61932	-0.038854	148.7
35	Dicotyledoneae	Cactaceae	0.98813	0.57251	0.090608	147.12
33	Dicotyledoneae	Compositae	1.0741	0.70726	-0.034657	148.65
38	Dicotyledoneae	Orobanchaceae	1.12	0.54393	0.26726	144.97
36	Monocotyledoneae	Palmae	1.1222	0.63488	0.12691	146.68
27	Monocotyledoneae	Iridaceae	1.3429	1.0491	-0.30178	151.9
34	Monocotyledoneae	Gramineae	1.4002	0.84476	0.075894	147.3
30	Monocotyledoneae	Orchidaceae	1.4063	1.0551	-0.24784	151.25
31	Monocotyledoneae	Araceae	1.5174	1.012	-0.069152	149.07
43	Monocotyledoneae	Agavaceae	1.6207	0.4537	0.90941	137.13
41	Dicotyledoneae	Asteraceae	1.8795	0.67031	0.82863	138.12
40	Monocotyledoneae	Asparagaceae	2.0053	0.78802	0.76991	138.84
42	Dicotyledoneae	Ranunculaceae	2.0285	0.72517	0.8916	137.35
44	Monocotyledoneae	Hyacinthaceae	2.3635	0.69028	1.2814	132.6
45	Dicotyledoneae	Loranthaceae	2.3797	0.68478	1.3062	132.3
46	Monocotyledoneae	Commelinaceae	2.5322	0.64196	1.5258	129.62
48	Monocotyledoneae	Xanthorrhoeaceae	2.7036	0.4	2.0765	122.9
49	Monocotyledoneae	Asphodelaceae	2.8054	0.33968	2.2729	120.51
50	Monocotyledoneae	Alliaceae	2.9051	0.39078	2.2924	120.27
47	Monocotyledoneae	Amaryllidaceae	2.9085	0.5811	1.9975	123.86
51	Dicotyledoneae	Paeoniaceae	2.957	0.28164	2.5155	117.55
53	Monocotyledoneae	Aloaceae	2.9724	0.2203	2.627	116.19
52	Monocotyledoneae	Liliaceae	3.5678	0.63278	2.5757	116.81

Table 8: **Origination order**

Superphylum	T_{ori} (Ma)	G_{mean_log}	G_{sd_log}	G_{sp}	G_{max}	G_{min}
Diploblostica	560	-0.4731	1.095	-2.1898	1.1506	-2.8134
Protostomia	542	-0.10229	1.2158	-2.0083	4.1685	-3.912
Deuterostomia	525	0.87752	1.0869	-0.82636	4.8891	-2.8134
bryophyte	488.3	-0.63576	0.54685	-1.4931	2.0757	-1.772
pteridophyte	416	1.7359	1.6606	-0.86744	4.2861	-2.4079
gymnosperm	359.2	2.8263	0.46055	2.1043	3.5835	0.81093
angiosperm	145.5	0.96878	1.2681	-1.0193	5.0252	-2.8134
Protist		-1.5532	1.6488	-4.1381	2.9755	-7.3475
Eubacteria		-5.8238	0.57889	-6.7313	-4.5865	-8.7269
Archaea		-6.02	0.50451	-6.811	-4.7404	-6.9616